Mineralium Deposita
https://doi.org/10.1007/s00126-026-01432-9

ARTICLE

Authigenic grey monazite from ordovician metasediments of the Iberian massif: the Matamulas placer

S. García de Madinabeitia[1] · A. Beranoaguirre[2,3] · P. Martínez[1] · R. Castroviejo[4] · E. Ortega[5] · F. Bastida[6] · E. W. G. Hellebrand[7] · E. Burkhalter[8] · J.I. Gil Ibarguchi[1,9]

Received: 3 June 2025 / Accepted: 31 December 2025

Abstract

Authigenic nodular monazite occurs in dark, Middle Ordovician, low-grade metapelites of the Central Iberian and West Asturian-Leonese Zones of the Iberian Massif. Erosion of monazite-bearing slates and phyllites, and short-range transport resulted in localised recent alluvial deposits rich in millimetre-size monazite, of which the Matamulas site, within the Central Iberian Zone, represents one of the most extensive and potentially exploitable placer-type accumulations of Th-poor grey monazite in western Europe. Nodular monazite from the Matamulas area depicts spheroidal or triaxial ellipsoid shapes and is mostly greyish, although it may display different surface colours from yellow to black. The nodules contain abundant silicate (quartz, feldspar, white mica, chlorite, zircon) and Fe oxides-hydroxides, organic matter, rutile and Mn oxide inclusions, generally oriented at random or showing orientations related to original bedding anisotropy. Nodular monazite displays concentric optical zoning, continuous or oscillatory, associated with the abundance and nature of inclusions. Chemical zoning is typically progressive, with cores enriched in medium and heavy rare earth elements (REE), and rims rich in light REE (La-Ce). Substitution of Pr by La-Ce is decoupled from that of elements with smaller ionic radii. Thorium contents are low (estimated mean 0.16 wt % ThO_2) and irregularly distributed across the monazite nodules. The increased concentration of phyllosilicate and other inclusions toward nodule rims, the sparse occurrence of twinning and the observed chemical zoning suggest progressive recrystallisation and refining from precursor gels or cryptocrystalline aggregates, facilitated by localized fluid-assisted element mobility during nodule growth. U-Pb dating of monazite yields an Early Devonian age of ca. 400 Ma, significantly older than the Upper Carboniferous age of regional metamorphism and tectonic foliation in the host metasediments. The age obtained, together with their non-oriented growth within specific levels of the sedimentary pile, indicates that the process of formation of nodular monazite took place through diagenesis or burial metamorphism. Although nodular monazite is absent from equivalent stratigraphic units in more internal zones of the Iberian Massif, its occurrence over a broad area of western Europe warrants further exploration for placer-type monazite deposits analogous to those at Matamulas in comparable geomorphological settings.

Keywords Rare earth elements · Grey monazite · Ordovician · Iberian massif · U-Pb age · LA-ICP-MS

Editorial handling: F. Tornos

✉ S. García de Madinabeitia
sonia.gdm@ehu.eus

1 Dpto. Geología, Universidad del País Vasco UPV/EHU, Bilbao 48080, Spain

2 Karlsruher Institut für Technologie, Angewandte Geowissenschaften, Adenauerring 20b, Karlsruhe, Germany

3 Institut für Geowissenschaften, Goethe-Universität Frankfurt, Altenhöferallee 1, Frankfurt am Main, Germany

4 Dpto. Ingeniería Geológica, E.T.S. Ingenieros de Minas, Universidad Politécnica de Madrid, Madrid 28003, Spain

5 Formerly at Minas de Almadén y Arrayanes S.A. (MAYASA), Almadén, Ciudad Real 13400, Spain

6 Dpto. Geología, Universidad de Oviedo, Oviedo 33005, Spain

7 Faculty of Geosciences, Utrecht University, Geolab, Utrecht 3584 CB, Netherlands

8 ecoNatura, Canillas 4, Madrid 28002, Spain

9 Servicio General de Geocronología y Geoquímica Isotópica-SGIker, Universidad del País Vasco UPV/EHU, Bilbao 48080, Spain

Published online: 26 January 2026

Introduction

Rare-earth element (REE) orthophosphates ($LnPO_4$) occur in nature with two different crystal structures: tetragonal xenotime (Ln = Y, Tb-Lu), for the heavy rare earths (HREE), and monoclinic monazite (Ln = La-Gd), for the light rare earths (LREE). The monazite group represents one of the principal REE ore minerals. Its general formula (Ce, La, Nd, Th)PO_4, reflects extensive solid solution with cheralite [(Ca, Ce, Th)(P, Si)O_4] and variable incorporation of the huttonite component ($ThSiO_4$), which can exceed 30 mol % (Boatner 2002; Förster and Harlov 1999). Two main varieties of monazite are recognised: yellow monazite and grey or dark monazite (Rosenblum and Mosier 1983).

Yellow monazite typically forms during igneous processes and medium- to high-grade regional metamorphism and, less frequently, through hydrothermal or metasomatic events (Harlov 2015; Santos et al. 2018 and references therein). Most yellow monazite crystals are elongated along the c-axis, display well-developed cleavage and are rich in Th and U, with average ThO_2 contents exceeding 7 wt % (Rosenblum and Mosier 1983). Values as high as 21 wt % ThO_2 and 8 wt % UO_2 have been reported in Variscan granites (Förster 2018). Yellow monazite, together with bastnäsite, constitutes the main REE ore in the world-class Bayan Obo (China) deposit (Ling et al. 2013). It is also a major REE resource in the heavy-mineral sands and placers of Australia, India, Madagascar, Brazil and South Africa, among other sites (Overstreet 1967; Rosenblum and Mosier 1983). However, both primary and secondary deposits commonly pose environmental concerns due to their high abundance in radionuclides of the Th and U decay series (Mohanty et al. 2004; Veerasamy et al. 2021). As a result, several authorities have restricted or prohibited mining of beach-sand monazite and imposed strict regulations on monazite stockpiles and tailings.

Grey (dark) monazite differs markedly from the yellow variety. First reported by Zemel (1936), it remained rarely documented until the systematic description by Rosenblum and Mosier (1983); notably, the comprehensive monazite review by Overstreet (1967) did not include it. Grey monazite occurs as scattered nodules within weakly metamorphosed sedimentary formations and as detrital grains in stream sediments or placers worldwide (e.g., Lazareva et al. 2018; Rosenblum and Mosier 1983; Tuduri et al. 2023 and references therein). The presence of grey monazite in its source rocks was first recognized in the 1970 s (Donnot et al. 1973). The nodules, typically several millimetres in size, display an ellipsoidal shape and range in colour from pale grey to nearly black. Their subcrystalline texture and rounded morphology can cause confusion with shale or schist fragments in the heavy fraction of panning concentrates. Their origin is unclear and several hypotheses have been proposed (review in Zi et al. 2024). Unlike yellow monazite, grey monazite is typically enriched in LREE and MREE, and very poor in Th (<1 wt % ThO_2; Rosenblum and Mosier 1983) and U (e.g. < 0.01 wt % UO_2 in Brittany; Tuduri et al. 2023). Consequently, grey monazite represents a potentially attractive REE source owing to its low radioactivity and minimal environmental impact.

However, known accumulations in placers contain relatively low ore grades, e.g. up to 1000 g/t in Belgium (Cobert et al. 2015) and 800 g/t in Brittany (Tuduri et al. 2023), with even lower contents in the primary host rocks. The small size and scattered distribution of these deposits have so far precluded economically viable exploitation, and most occurrences are regarded as of limited resource potential.

In this context, renewed exploration in the Campo de Montiel area (Ciudad Real, Spain) has revived interest in grey monazite deposits. Preliminary surveys by the Spanish national company ADARO in the early 1990 s (Kremenetski et al. 1993) and subsequent investigations by Quantum Minería have revealed promising occurrences. Published information from the Matamulas mining research permit there (Vergara Espuelas 2015, 2019) indicates that alluvial Quaternary grey-monazite placer deposits extend along a 9-km-long valley, 0.5–2 km in width and up to 2.5 m in depth. The monazite, derived from surrounding low-grade Ordovician metasediments, comprises approximately 1 wt % of the Quaternary sedimentary fill. Concentrations locally reach >3000 g/t, corresponding to inferred and indicated resources of 46,000 t and 24,000 t of total rare earth oxides (TREO), respectively. Continued exploration in adjacent alluvial areas may significantly increase these estimates. Given the strategic importance of REEs in modern technologies and their rising global demand (e.g., European Commission 2023), the Matamulas placer deposit has the potential to become a major resource of low-radioactivity REE ore.

This study revises the main characteristics of nodular grey monazite within Ordovician metasediments of the Iberian Massif, with special emphasis on the geochemistry and geochronology of monazite from Matamulas. Our results aim to improve the assessment of the deposit and to provide clues for future exploration of REE resources hosted in similar settings.

Geological background

The Matamulas area lies within the Schist-Greywacke Domain of the Central Iberian Zone (CIZ) of the Variscan Iberian Massif (Martínez Catalán et al. 2004; Fig. 1a). The studied sector forms a band of Quaternary deposits located

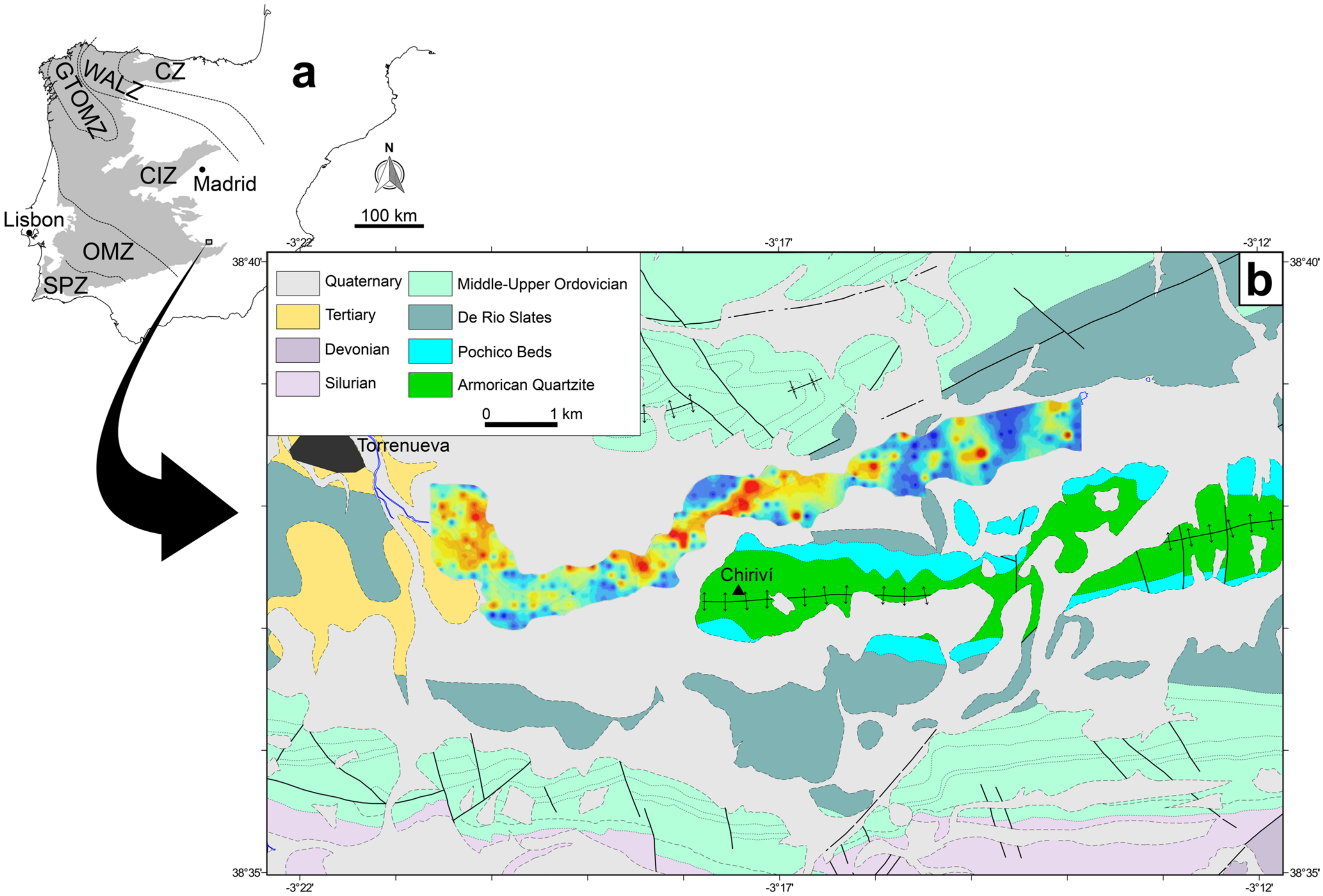

Fig. 1 **a** The Iberian Massif (in grey) of Spain and Portugal showing its main subdivisions or tectonic zones. CZ: Cantabrian Zone; WALZ: West Asturian-Leonese Zone; GTOMZ: Galicia-Trás-os-Montes Zone; CIZ: Central Iberian Zone; OMZ: Ossa-Morena Zone; SPZ: South-Portuguese Zone. **b** Geological sketch map of the Matamulas area, east of Torrenueva, simplified from the Geological map of Spain, scale 1:50,000 sheet 838 (Spanish Geological Survey, IGME 2016b). Variations in monazite concentration are showm from richer (red) to poorer (blue) areas within the the explored zone (Vergara Espuelas 2015, 2019)

north of Chiriví hill (965 m a.s.l.), representing the western continuation of the Cabeza de Buey range, east of Torrenueva (Ciudad Real province, Spain; Fig. 1b). In current reconstructions of the Variscan Foldbelt of Europe (e.g., Martínez Catalán et al. 2021), the CIZ correlates with the Central Armorican Domain and the Pyrenean Axial Zone, both of which also host occurrences of nodular grey monazite (Lacomme et al. 1993; Tuduri et al. 2023 and references therein).

The stratigraphic succession in the Matamulas area comprises, from base to top, a ca. 500 m thick quartz arenite (orthoquartzite) of Lower to Middle Ordovician age (Floian-Darriwilian), regionally referred to as the Armorican Quartzite. This formation is one of the most characteristic lithostratigraphic units of the Schist-Greywacke Domain, as it forms major ridges and defines the most conspicuous Variscan folds at the regional scale. Overlying this unit is a ca. 100 m thick succession of quartzites, sandstones and black slate, richer in quartzitic facies at the base and progressively more pelitic upward. Known as the Pochico Beds, this sequence forms a fringe around the Armorican Quartzite core (Fig. 1b) and morphologically represents the transition from uplifted areas to the depressions generated by the overlying slates.

The Pochico Beds locally contain dark metasandstone layers enriched in U- and Th-bearing minerals, mostly zircon and rutile but also yellow monazite, titanite and apatite. These horizons, interpreted as paleoplacers and historically termed 'radioactive' or 'uraniferous quartzites' were studied in detail by the Spanish Nuclear Energy Board (Alía Medina 1962). The Pochico Beds are overlain by up to 700 m of grey and black Middle Ordovician (Darriwilian) slates known as the De Río Slates. The source rocks for the monazite nodules, first reported by Kremenetski et al. (1993), correspond to the uppermost slate layers of the Pochico Beds and the basal black slates of the De Río unit. The depositional environment is interpreted as a low-energy siliciclastic platform, influenced toward the top of the sequence by basic to intermediate volcanic activity (IGME 2009, 2016b). The monazite-bearing black slates of consist primarily of quartz, chlorite and micas, with minor clastic components (quartz, K-feldspar, plagioclase, micas and volcanic lithic fragments).

Structurally, the area forms an E–W-trending anticline with the Armorican Quartzite at its core (Fig. 1b). This geometry is associated with the development of a slaty cleavage (S_1) in the overlaying slates and a rough cleavage in the sandstones and quartzites. The S_1 cleavage is subvertical and verges slightly to the NE or SW. Its development is considered post-Serpukhovian (Upper Carboniferous), which is the age of the younger Culm sediments affected by the main D_1 Variscan deformation.

The monazite-bearing placer deposits rest unconformably on the Paleozoic metasediments exposed north and west of the Cabeza de Buey range. The local Variscan structure is largely concealed by Plio-Quaternary cover but can be interpreted as gentle folds intersected by transverse to oblique faults (IGME 2016b). This structural configuration produced a landscape in which resistant Ordovician quartzites and sandstones (mainly the Armorican Quartzite) form topographic highs, whereas the less competent Pochico Beds and the De Río Slates, both hosting grey monazite, favoured the development of depressions, including the valley where the Matamulas deposit accumulated (Vergara Espuelas 2015, 2019). Within this valley, fluvial, colluvial and lateral inputs from alluvial and piedmont fans produced detrital sequences ranging from pebbles to clays. Weathering and erosion of the monazite-bearing source rocks released nodules that accumulated to form the present placer deposit.

Materials and methods

Monazite-bearing sand from the Matamulas area was wet-sieved into five granulometric fractions: >2 mm, 2–1.2 mm, 1.2–0.4 mm, 0.4–0.1 mm, and <0.1 mm. For the fractions between 2 and 0.1 mm, gravimetric separation was employed to obtain barren, mixed, and concentrate products. Seventeen polished petrographic thin sections from these fractions were examined by optical microscopy under transmitted and reflected light. In addition, three polished epoxy mounts of the concentrate fraction were analysed using an automated mineral analysis system (MLA) based on a scanning electron microscope equipped with energy-dispersive X-ray spectroscopy (SEM-EDX) to estimate grain size distribution and modal proportions of mineral constituents within the nodules.

A 12 g subsample of the concentrate was inspected under a stereomicroscope to document surface textures and colour variations. Four aliquots of monazite concentrate were analysed quantitatively by X-ray fluorescence (XRF) and inductively coupled plasma-atomic emission spectrometry (ICP-AES). Two polished petrographic thick (≥80 µm) sections, containing a total of 75 monazite grains of different colours, were prepared for quantitative spot analysis of monazite and its mineral inclusions by electron microprobe (EPMA), and by laser ablation-based techniques. Six of these grains, selected to represent the full range of surface colours, were further examined for detail chemical characterisation by laser ablation-quadrupole mass spectrometry (LA-Q-ICP-MS).

U-Th-Pb geochronological analyses were performed on three monazite grains of different colours by laser ablation coupled to a sector-field mass spectrometer (LA-SF-ICPMS). Details on analytical protocols, instrument parameters and the laboratories involved are provided in the Supplementary Information.

In addition to the samples from the Matamulas placer, we examined numerous monazite-bearing samples from Middle Ordovician rocks and panned sediments from various parts of the Iberian Massif. Although these were not investigated in the same detail as the Matamulas material, they are included in the discussion.

Results

Petrographic description

The nodular monazite of Matamulas has been greatly liberated from the matrix through erosion and natural detrital concentration processes. As a result, although a mixed fraction was obtained gravimetrically, composite grains containing both monazite and other minerals are rare and nearly absent in the concentrate fraction (Fig. 2a). Some of the composite grains display irregular outlines, being locally broken and cemented by pelitic material. The barren and mixed fractions share similar mineral assemblages, although in different proportions. In addition to monazite, both contain phyllosilicates (clay minerals, muscovite, biotite, chlorite), quartz and iron oxides (goethite, hematite or limonite), as well as organic matter and Mn oxides. Carbonates, feldspars, rutile, anatase, leucoxene, zircon, apatite and pyrite pseudomorphs or vestiges of it (Supplementary Fig. 1) occur as accessories making < 5 vol %.

Liberated monazite in the concentrate fraction was initially described in Castroviejo (2023). Additional information is presented herein. Nodular monazite exhibits micropitted surface (Fig. 2a) and occurs in the submillimetre- to millimetre-sized range (0.2 to > 2 mm), with approximately 80% of the nodules exceeding 1.1 mm. Based on surface colour, the nodules are classified as yellowish, greyish or reddish; the yellowish variety should not be confused with the Th- and U-rich yellow monazite mentioned in the

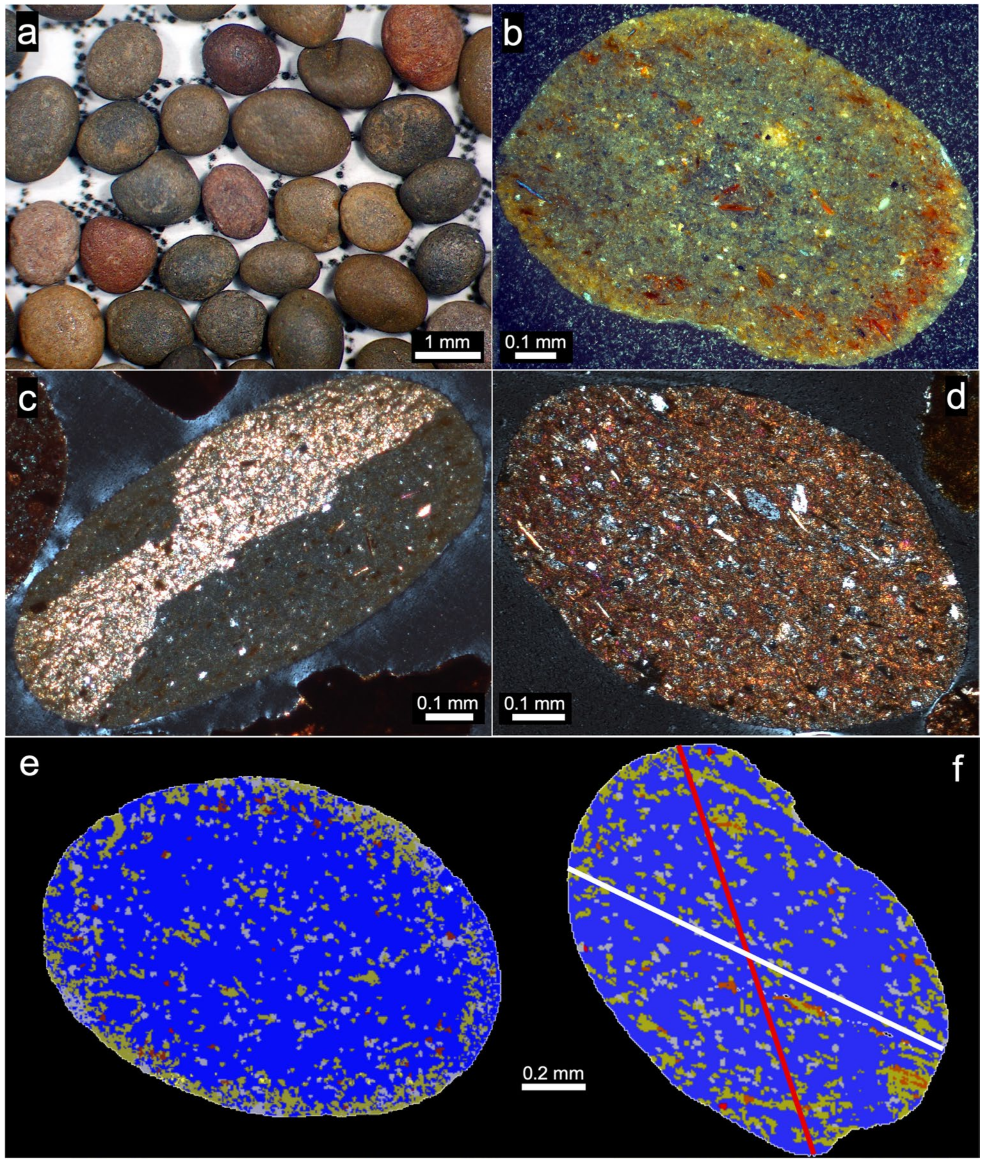

Fig. 2 Representative pictures of nodular grey monazite from the Matamulas placer deposit. **a** Detail picture of spheroidal to ellipsoidal grains showing colour variations and pitted surfaces. **b** Reflected-light, cross-polarized (XPL) image of kidney shaped monazite showing aligned and unoriented inclusions of quartz, phyllosilicates and opaques, as well as bright reddish-brown internal reflections due to limonite. **c** Transmitted-light, XPL image of an elongated monazite grain showing incipient cyclic twinning and inclusions aligned parallel to the major axis of the elliptical section. **d** Transmitted light, XPL image of elongated grain of rich in oriented inclusions parallel to the major axis of the elliptical section. **e**-**f** Electron microscopy images using the MLA system. **e** Increased abundance of inclusions toward grain rims of the nodules (blue: monazite; grey: quartz; yellowish: phyllosilicates; red: oxides-hydroxides). **f** Bean-shaped monazite displaying oriented inclusions (white line) oblique to the inferred major axis (red line)

Introduction. A stereomicroscopic examination of ca. 1600 liberated grains (Fig. 2a; Supplementary Fig. 2) yielded the following proportions: greyish, ca. 62.5%; yellowish, ca. 22% and reddish, ca. 15.5%.

The nodules show mostly uniaxial oblate to triaxial flattened ellipsoidal shapes (terminology after Ramsay 1967) and, less commonly, kidney-, bean-like, or irregular forms (Fig. 2b and f). In thin section, greyish and yellowish monazite grains appear rather similar, whereas reddish nodules are distinct due to limonite impregnation that, in extreme cases, may render the nodule opaque. Greyish and yellowish varieties commonly show optical zoning with darker cores and lighter rims, although the pattern may be reversed or display multiple cycles (Supplementary Figs. 3a, 3b). Zoning is poorly discernible in reddish nodules. Nodular monazite is weakly anisotropic, but interference colours are almost completely masked by the colour of the mineral (transmitted light) and by the abundant internal reflections that may acquire various reddish-brown shades due to limonite impregnation (reflected light, Fig. 2b). Cleavage is absent. Incipient cyclic twinning is sometimes recognized under cross-polarised light (XPL) (Fig. 2c and Supplementary Fig. 4).

The nodules contain abundant mineral inclusions ranging from subspherical micro-inclusions of limonite (possibly pseudomorphs of framboidal pyrite) to subhedral phyllosilicates $\geq$ 100 µm (Figs. 2b-f). Included minerals comprise irregular to subrounded quartz (> 5 vol %), white mica (3–4 vol %), chlorite or chloritized biotite (2–3 vol %) and opaques (goethite, limonite, hematite and minor Mn oxides; each < 1 vol %). Rutile, zircon, feldspar and other accessory phases are very rare (< 0.1 vol % overall) (estimates by MLA system). The inclusions, generally distributed at random, show often contrasting patterns of density with a clear increase near rims (Fig. 2e). Although many inclusions are unoriented, aligned phyllosilicates and, less frequently, opaques and quartz also occur. Oriented inclusions are typically parallel (Figs. 2c-d) or slightly oblique (Fig. 2f) to the major axis of the elliptical sections of the nodules.

Bulk ICP-AES analysis

Quantitative analyses of whole nodules from four monazite fractions were obtained using two techniques: X-ray fluorescence following alkali fusion, and four-acid digestion (HNO_3, $HClO_4$, HF, HCl) coupled with ICP-AES. Results for the analysed fractions are broadly consistent and are presented in Table 1 of the Supplementary Information. The results show high contents of Pr (average $Pr_2O_3 = 3.37$ wt %), Nd (average $Nd_2O_3 = 13.08$ wt %), Sm (average $Sm_2O_3 = 2.61$ wt %) and Eu (average $Eu_2O_3 = 0.34$ wt %). ThO_2 contents are 0.16 wt % as average. Relatively elevated values of Si (average $SiO_2 = 9.66$ wt %) and other elements such as Al or Fe, along with substantial loss on ignition values (ca.1.20 wt %), likely reflect the abundance of quartz and phyllosilicate inclusions in the analysed fractions.

EDX and electron microprobe results

Compositional images of grey monazite by EDX (MLA system) revealed continuous zoning of La, with enrichment towards the rims, as well as minute, unidentified inclusions distinctly richer in this element (Fig. 3a). Irregular zones of Th enrichment were observed in the inner areas of some nodules (Fig. 3b). Wavelength-dispersive X-ray spectroscopy (WDX) via EPMA confirmed this REE chemical zonation: rims were enriched in La and Ce (Fig. 3c and Supplementary Fig. 6a), whereas cores were enriched in Nd, Sm and Gd (Figs. 3d-e and Supplementary Fig. 6b). The zoning is concentric and predominantly continuous, though oscillatory variations were noted for Nd and Pr (Fig. 3d and Supplementary Fig. 6c, respectively). Other major and minor elements (in the monazite crystal lattice) like P, Y, Si, Al or K did not display zonation and are mainly associated with inclusions (Supplementary Fig. 7). Thorium concentrations range from 0.01 to 0.40 wt % ThO_2, with over 40% of the measurements below the detection limit; mean uranium content is 0.05 wt % UO_2.

Analyses of monazite inclusions (Tables 3, 4, 5, 6 and 7 in Supplementary Information) showed that quartz (>50 µm) did not show distinctive compositional features. Phyllosilicates of similar size were difficult to analyse due to pervasive alteration to clay minerals. The presence of biotite, tentatively identified under optical microscopy

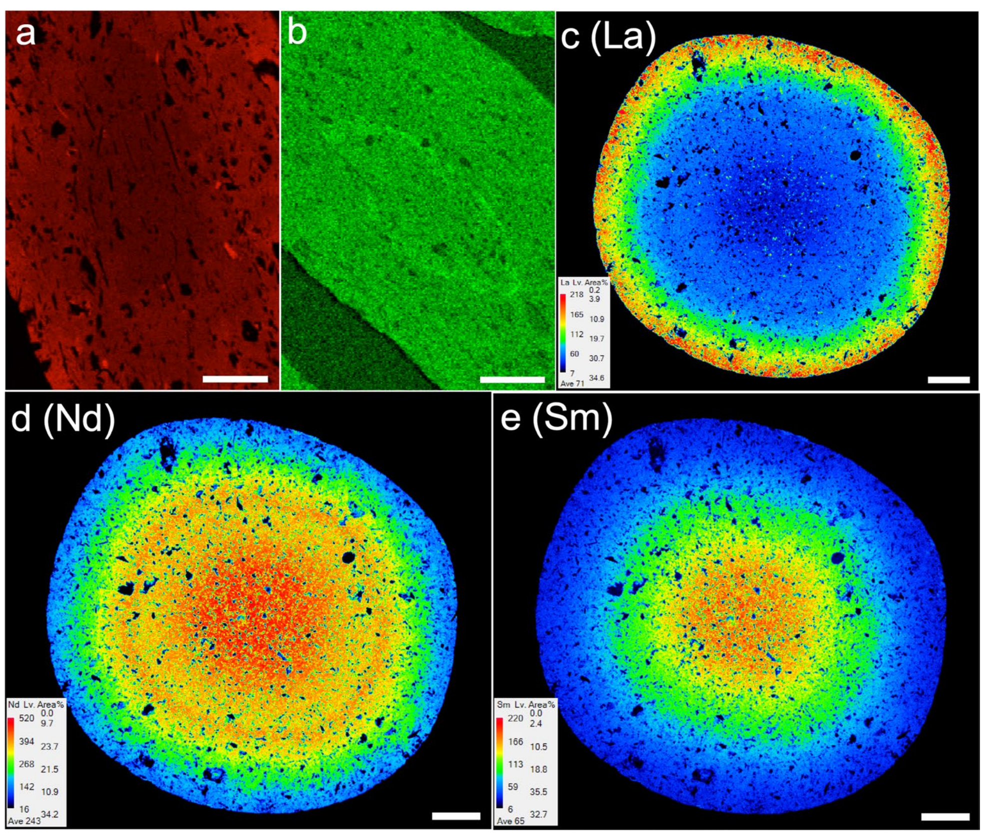

Fig. 3 **a-b** EDX compositional images (MLA system) of nodular monazite from Matamulas; scale bar: 100 µm. **a** Continuous La zoning with rimward enrichment and minute La-rich inclusions. **b** Irregular Th-enriched zone in the inner part of the nodule. **c-e** WDX compositional images (EPMA); scale bar: 200 µm. **c** Continuous La enrichment from core to rim. **d-e** Nd and Sm enrichment at grain cores (yellow/red), decreasing towards rims (blue); Nd shows a recurrent zone midway between core and rim

(Fig. 2b and e), could not be confirmed because of intense chloritization. Potassium white micas were more amenable to analyses and exhibited a variety of compositions. They have been separated into two groups based on their Si contents and interlayer charges. This allows to differentiate a group of common muscovites, which have a small proportion of vacancies in alkali sites, and a group of illitic muscovites which have lower alkali contents and are richer in Si and paragonite molecule than the former. Most common muscovites have high interlayer charge, with K as the main interlayer cation, albeit with significant and variable paragonite (X_{Na} = 0.14; 2SE = 0.06) and phengite (Si_{apfu} = 3.006–3.258) components. Chlorite inclusions are rich in Fe^{2+} (Fe/Fe + Mg = 0.69–0.96) with highly variable Si_{apfu} (4.3–7.2) and relatively high K_2O (average 1.71 wt %), consistent with derivation from biotite alteration. They are classified as brunsvigite to pseudothuringite (Hey 1954). Other phyllosilicates could not be reliably identified due to small grain size and low analytical totals; some, composed of Si and Al with high Fe, are tentatively assigned to iron-rich halloysite or related clays. Opaque minerals are abundant but generally too small for precise analysis. Their variably compositions likely reflect mixed oxide-hydroxide hydrate alteration products and intergrowth with silicates. Nonetheless, relatively high contents of Si, Al and P, coupled with low analytical totals indicative of significant H_2O contents, suggest that most of them correspond to goethite (Pownceby 2019).

Laser ablation ICP-MS composition of monazite

Six representative nodular monazite grains, two of each colour, were analysed for multielemental concentrations using LA-Q-ICPMS. A total of 324 spot analyses were obtained, with 43 to 72 measurements per grain along traverses across the nodule sections (Table 1, Supplementary Information). No systematic compositional differences were observed among grains of different colour; however, substantial differences exist between cores and rims. Boxplots in Fig. 4a, grouped by analysis location (core vs. rim) summarize this trend.

REE concentrations display a concentric zonation, with lower LREE contents in the cores (La_2O_3_min = 3.6 wt %; Ce_2O_3_min = 17.3 wt %) and pronounced enrichment towards the rims (La_2O_3_max = 25.1 wt %; Ce_2O_3_max = 35.4 wt %). Conversely, the cores are enriched in Nd, Sm, Eu and Gd (Nd_2O_3_max = 26.5 wt %; Sm_2O_3_max = 11.5

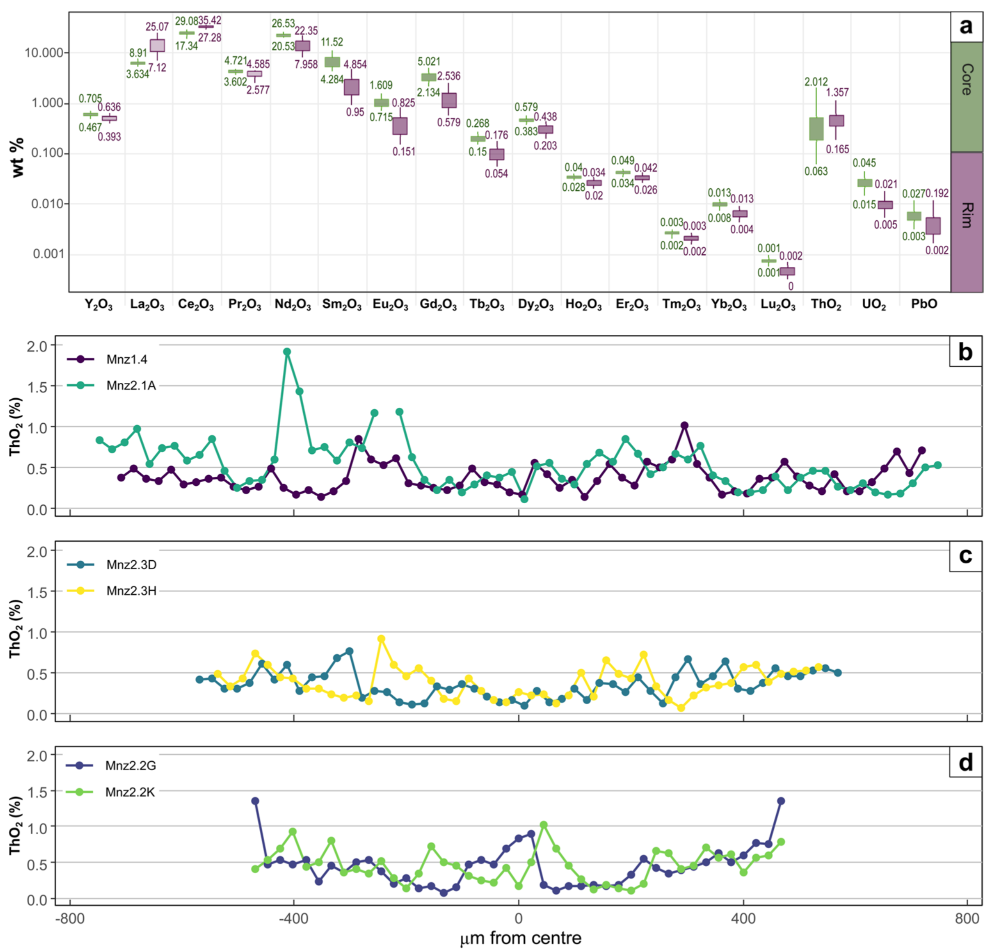

Fig. 4 **a** Boxplots of LA-Q-ICP-S analyses grouped by location (cores vs. rims). Boxes represent the range between the first and third quartiles; whiskers extend from the box to the minimum and maximum values excluding outliers. Numerical values indicate the minimum and maximum measurements for each variable. **b-d** Variations in Th content along traverses in monazite of different size and colours: **b** Grey; **c** Yellowish; **d** Reddish. X axis: spot locations along diametral traverses. Y axis: ThO_2 concentration (wt %). The spikes occur irrespective of colour or spot position, with enrichment appearing at any point from core to rim

wt %; Eu_2O_3_max = 1.6 wt %; Gd_2O_3_max = 5 wt %) relative to rims (Nd_2O_3_min = 8 wt %; Sm_2O_3_min = 1 wt %; Eu_2O_3_min = 0.15 wt %; Gd_2O_3_min = 0.6 wt %).

Thorium and uranium do not exhibit systematic zonation along the core-rim traverses. Heterogeneous distribution of Th within individual nodules, attested by irregular Th-enriched zones identified by the EDX (Fig. 3a-b), are confirmed as spikes of elevated Th content at various positions along the traverses, independent of grain size or colour (Fig. 4b and d). Including these spikes, the average Th content is 0.43 wt % ThO_2, whereas the mean UO_2 concentration is 0.02 wt %.

U-Pb geochronology by LA-SF-ICPMS

Three representative nodular monazite grains, one of each colour, were analysed for U-Pb geochronology using LA-SF-ICPMS. Individual results are reported in Table 2 of the Supplementary Information and plotted in Fig. 5. The dates obtained, anchored to the Stacey and Kramers (1975) $^{207}Pb/^{206}Pb$ values at 400 Ma, are 401.8 ± 2.3/6.3 Ma (n = 48; MSWD = 1.73) for the reddish monazite, 398.8 ± 1.7/6.1 Ma (n = 50; MSWD = 1.69) for the yellowish monazite and 399.1 ± 2.3/6.2 Ma (n = 47; MSWD = 1.57) for the grey monazite. Integration of the whole U-Pb data set in a single calculation yields an Early Devonian age of 399.8 ± 1.3/6.0 Ma (n = 145; MSWD = 1.71).

Discussion

Distribution of nodular grey monazite in the Iberian Massif

Erosion of low-grade metasediments of Middle Ordovician age, particularly dark slates of the uppermost Pochico Beds and the De Río Slates, led to the formation of extensive Quaternary placer deposits of grey monazite in the Matamulas area. The alluvial deposits occur within the core of an open syncline, bordered by Armorican Quartzite reliefs (locality 2 in Fig. 6). The preservation of slate fragments attached to some monazite grains suggests that the placers are proximal to their source rocks. The present relief likely stabilized shortly after the main Variscan deformation, as indicated by discordant Stephanian deposits and reddening of Ordovician sediments observed in exploratory drillings in the nearby Puertollano coal basin (MAYASA, internal report; IGME 2016a).

Equivalent Middle Ordovician slates occur elsewhere in the CIZ, West Asturian-Leonese Zone (WALZ) and Cantabrian Zone (CZ) of the Iberian Massif (Fig. 6), regionally known as Luarca Slates or "slates with Calymene" due to fossil content. The lower part of the overlying Agüeira Formation, also Middle Ordovician and slate-rich, is considered together with these units (Fig. 6; Rodríguez Fernández et al. 2015). All these formations correspond to the more distal and deeper parts of an extensive Ordovician basin. Despite this widespread geological setting, nodular grey monazite has only been found in the CIZ and WALZ. The known areas of occurrence of nodular grey monazite related to Middle Ordovician rocks are revised below.

In the context of early explorations by ADARO in the 1970 s, igneous yellow monazite was found in the north of the central area of Los Pedroches batholith (Vaquero Nazábal 1976). Nodular grey monazite was also found in these studies, but it was not recognised as a different monazite variety until a few years later, when it was identified by XRD (Vaquero Nazábal 1979). Although the precise sample location was not addressed by these documents, it is likely to occur in alluvial deposits sourced from nearby Middle Ordovician metasediments. Thus, the site 1 in Fig. 6 is tentative.

Northwest of Matamulas, near Navas de Estena in the central sector of the Montes de Toledo (locality 3 in Fig. 6), nodular grey monazite has been found in situ within De Río Slates and, more rarely, in underlying Pochico Beds (Fig. 7a; Supplementary Figs. 8a, 8b). Monazite there occurs in the coarse-grain lenses intercalated within the shaly-sandy layers. Likewise, nodular monazite is very abundant in panned alluvial sediments, being the greyish nodules the most abundant (Fig. 7b). The grains appear in the field as millimetric bulges on tectonic foliation planes (S_1 parallel to S_0; Fig. 7a), pointing to monazite formation in specific levels of the stratigraphic sequence. The nodules are roughly oriented on the foliation planes (e.g., the four nodules marked with arrows in Fig. 7a). Thus, based on field data and textural relationships between the monazite grains and the S_1 cleavage (Figs. 7c-d), a pre-D1 origin can be inferred.

The presence of monazite within panned deposits near Alía (Cáceres, locality 4 in Fig. 6), with characteristics very similar to those of Montes de Toledo, suggests a direct correlation with the main source level of the Ordovician sequence, that is, with graphite-rich slates of Middle-Upper Ordovician age (Junta de Extremadura 2019). Our own observations include a campaign of collecting 30 surface samples from sediments in the live beds of streams in the vicinity of this location, which yielded monazite concentrations always below 150 ppm.

Similarly, at the northeast of this sector, in the Monfortinho area of Portugal (locality 5 in Fig. 6), minor amounts of grey monazite have been found at various localities in the magnetic fraction of alluvial sediments (Salgueiro et al. 2020). According to these authors, the source rock may be either the slates of the Neoproterozoic to lower Cambrian

Fig. 5 U-Pb results obtained by laser ablation-SF-ICP-MS on three nodules of monazite of different surface colours from the Matamulas placer deposit. Dates quoted with 2 sigma uncertainties

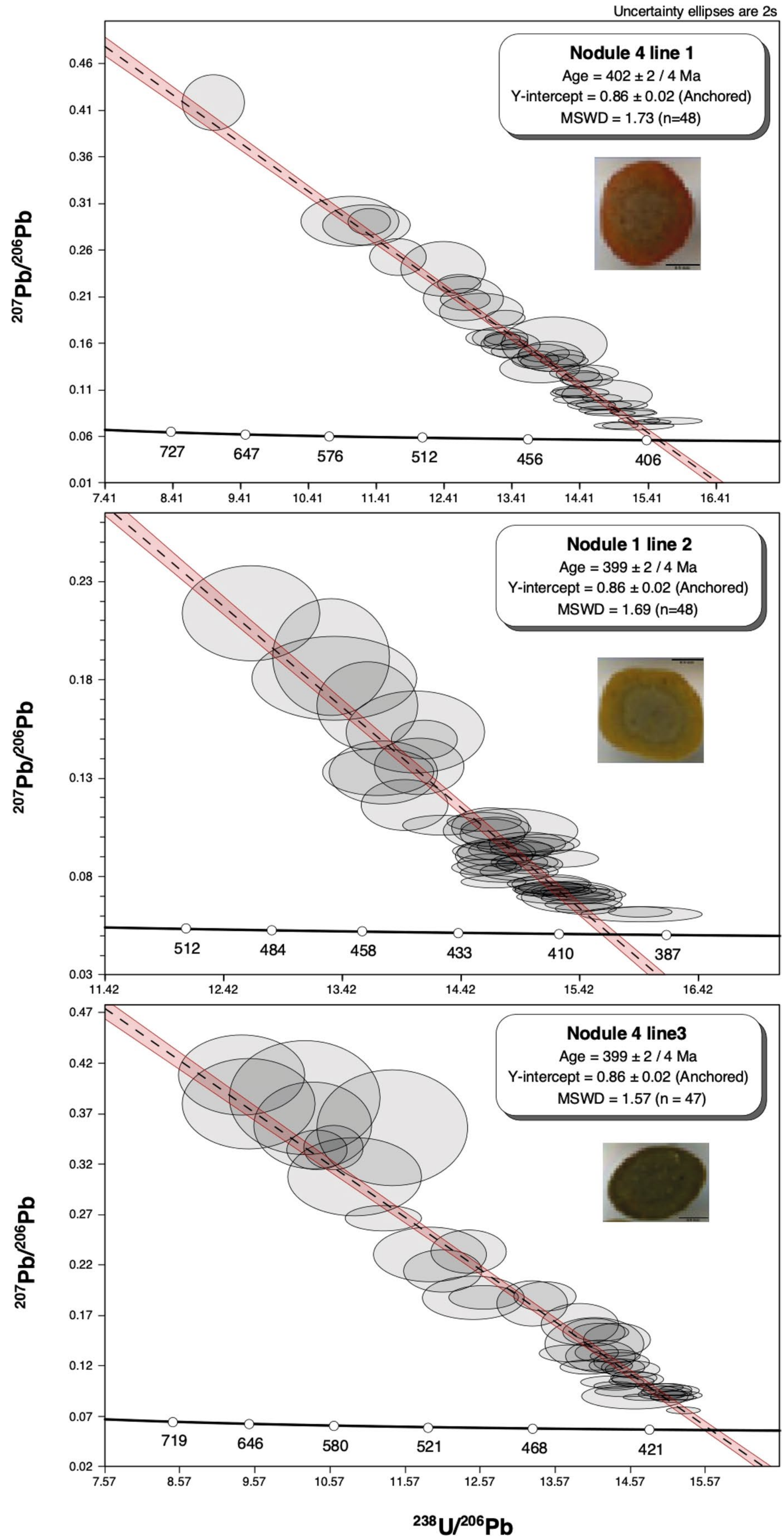

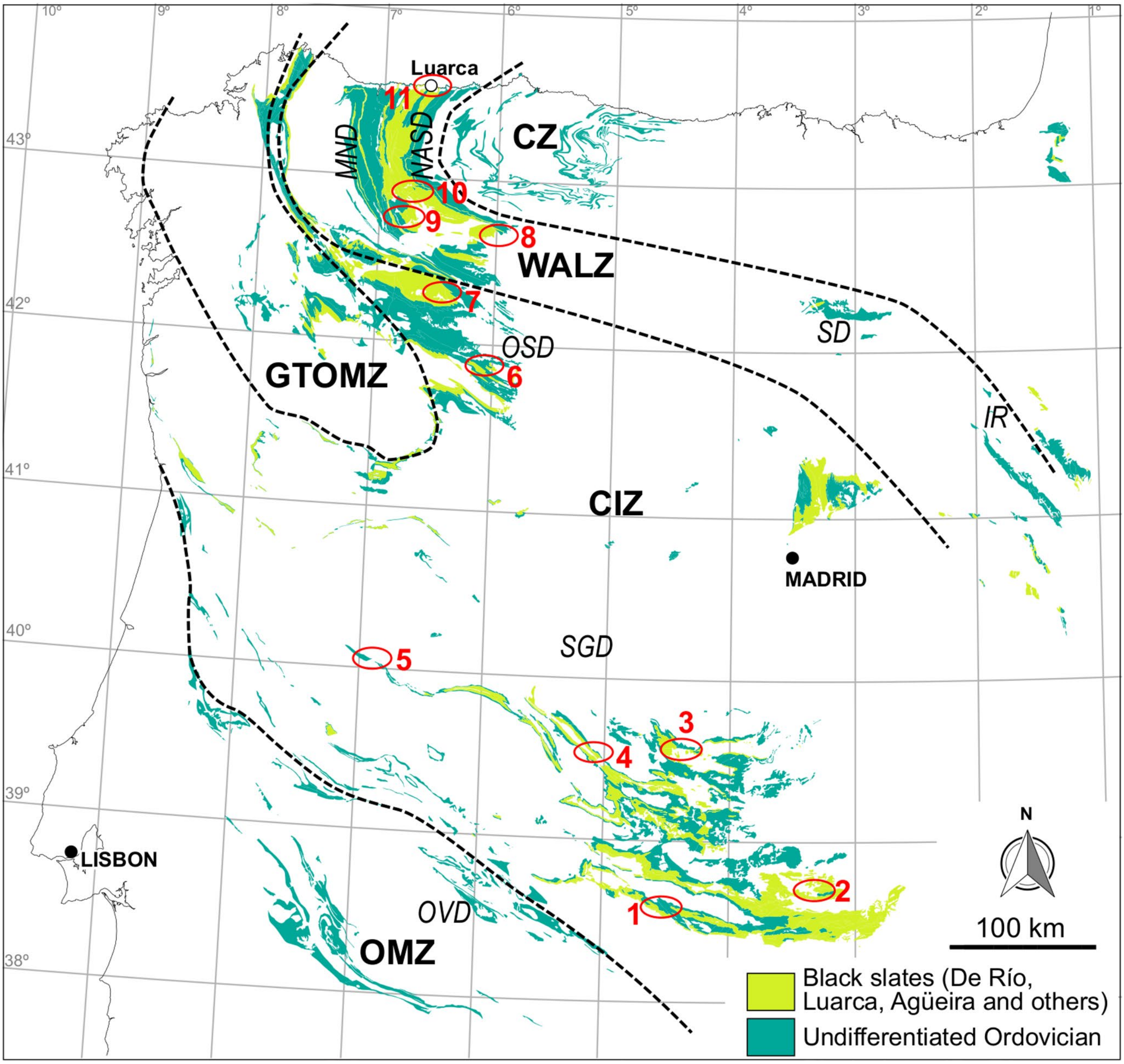

Fig. 6 Outcrops of Ordovician rocks within the Variscan Iberian Massif (Rodríguez Fernández et al. 2015) showing known areas (numbered red ellipses) containing in-situ or panned nodular grey monazite (see text for details). 1: Los Pedroches batholith; 2: Matamulas; 3: Montes de Toledo; 4: Alía; 5: Monfortinho and Penha García-Cañaveral syncline; 6: Alba and Tábara; 7: Truchas; 8: Monterrequejo stream; 9: Cúa river; 10: Anllarinos; 11: Luarca. Map after Rodríguez Fernández et al. (2015). CZ: Cantabrian Zone; WALZ: West Asturian-Leonese Zone; GTOMZ: Galicia-Trás-os-Montes Zone; CIZ: Central Iberian Zone; OMZ: Ossa Morena Zone; NASD: Navia-Alto Sil Domain: MND: Mondoñedo Nappe Domain; OSD: Ollo de Sapo Domain; SD: Sierra de la Demanda; IR: Iberian Ranges; SGD: Schist-Greywacke Domain; OVD: Obejo-Valsequillo Domain

Schist-Greywacke Domain or the centimetric quartzite layers within Middle Ordovician slates, equivalent of the U- and Th-rich dark metasandstones of the Pochico Beds. In view of the abundance of other U- and Th-bearing heavy minerals (zircon, rutile, xenotime, yellow monazite, ilmenite…) within the panned concentrates, we estimate that grey monazite might rather come from the pelitic levels of the Middle Ordovician units, as is the case for the Spanish sectors. Our own research to the north of the area studied by Salgueiro et al. (2020) revealed the presence of large nodules of grey monazite within alluvial sediments of the Penha García-Cañaveral Ordovician syncline depression, which would exclude an origin from rocks of the Neoproterozoic to lower Cambrian Schist-Greywacke Domain.

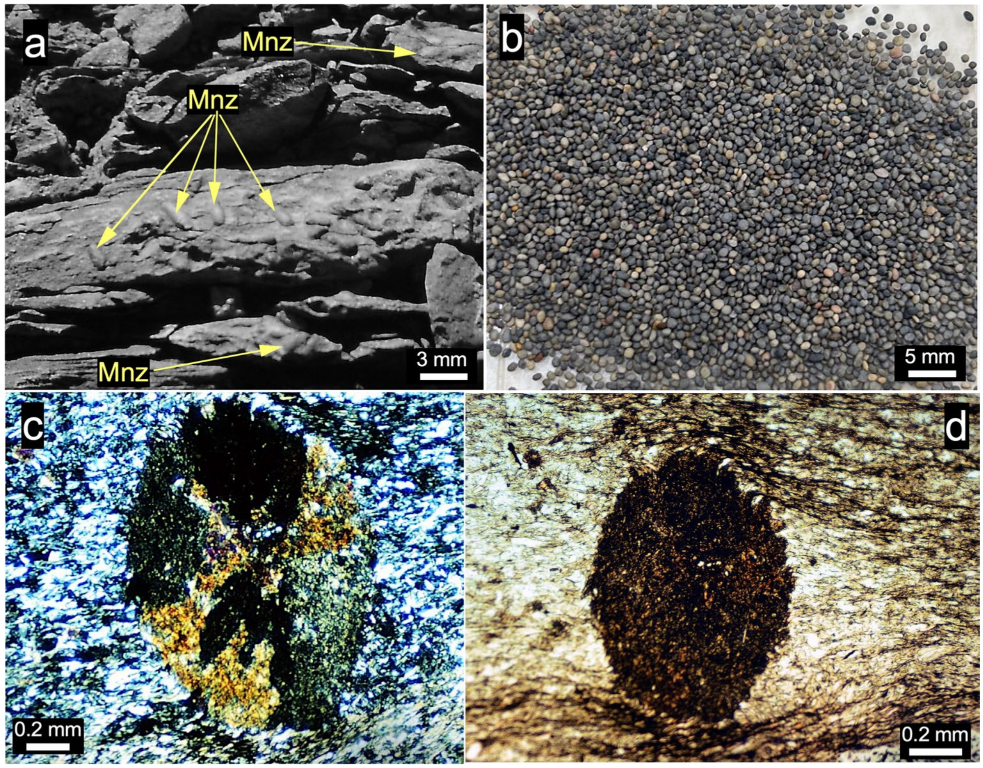

Fig. 7 Representative images of grey monazite from the Navas de Estena area (Montes de Toledo; locality 3 in Fig. 6). **a** Millimetre-scale nodular bulges on the surface of S_1 parallel to S_0 in Ordovician metalutite. **b** Batch of nodules showing predominantly greyish and yellowish grains. **c** Transmitted-light (XPL) image of nodule and host rock in thin section showing cyclic twinning and slight S_1 deflection. **d** Transmitted-light (PPl) image of nodule and host rock in thin section showing well-developed pressure shadows and S_1 deflection; note irregular rims prior to rounding during transport and erosion

Further north, in the province of Zamora, nodular grey monazite with similar surface features to those of Matamulas occurs in panned stream sediments of the Alba and Tábara areas (locality 6 in Fig. 6). Considering the regional geology of the area (González Clavijo 2006), the monazite would come from the Middle Ordovician slates outcropping along the northern limb of the Alcañices synform. Additionally, nodular monazite < 200 µm in size has also been reported within the very low-grade Middle Ordovician Luarca Slates of the Truchas syncline, just N of the Alcañices synform, at the northern fringe of the CIZ (locality 7 in Fig. 6). Lozano Letellier et al. (2023) proposed a syntectonic crystallisation of the monazite and interpreted the aligned mineral inclusions as a rotated foliation.

The WALZ represents the transition zone between the most internal areas of the Variscan Orogen (CIZ) and the external foreland and thrust belt (CZ, Fig. 6). In the south of the Navia-Alto Sil Domain (NASD in Fig. 6) of this Zone, nodular grey monazite was found during an exploration project by the IGME and ADARO. The most prolific areas for grey monazite exploitation were found in Quaternary deposits along the Monterrequejo creek and Cúa river (localities 8 and 9 in Fig. 6), where monazite contents up to 1500 and 600 g/m^3 were estimated, respectively. The source area for the grey monazite would have been the Ordovician slates of the Luarca and Agüeira Fms. outcropping in the vicinity. Vaquero Nazábal (1979) published the results of the study, pointing out the presence of nodular monazite up to 4.5 mm in size (0.5–1 mm on average). The study of samples taken in the same formations to the north of the area studied by ADARO has revealed the presence of nodular monazite along the slate belt (Fig. 8a and c and Supplementary Figs. 9a, 9b), from Anllarinos in the south (locality 10 in Fig. 6) to Luarca in the north (locality 11 in Fig. 6). The localised formation of monazite in the pelitic layers rich in organic matter adjacent to sandy ones is well displayed in Fig. 8a and may be abundant even at the thin section of scale (e.g., Fig. 8c). Nodular monazite in the Ordovician slates of the WALZ might likely have been misinterpreted by previous authors and identifying it as millimetre-size spherules and ellipsoids made of polyframboidal pyrite clusters.

Geochemistry

Previous geochemical studies of nodular grey monazite have focused on: (i) major and trace element bulk composition, and (ii) in situ analytical data (EDX, EPMA, LA-ICP-MS). Bulk analyses, typically performed by X-ray fluorescence (XRF), acid dissolution methods, or occasionally instrumental neutron activation analysis, are relatively rare (e.g., Burnotte et al. 1989; Cooper et al. 1983; Rosenblum and Mosier 1983). These approaches integrate the composition of the monazite host and its inclusions, often yielding elevated SiO_2, Fe and Al contents. Despite this, prior results consistently highlighted the distinctive chemistry of grey

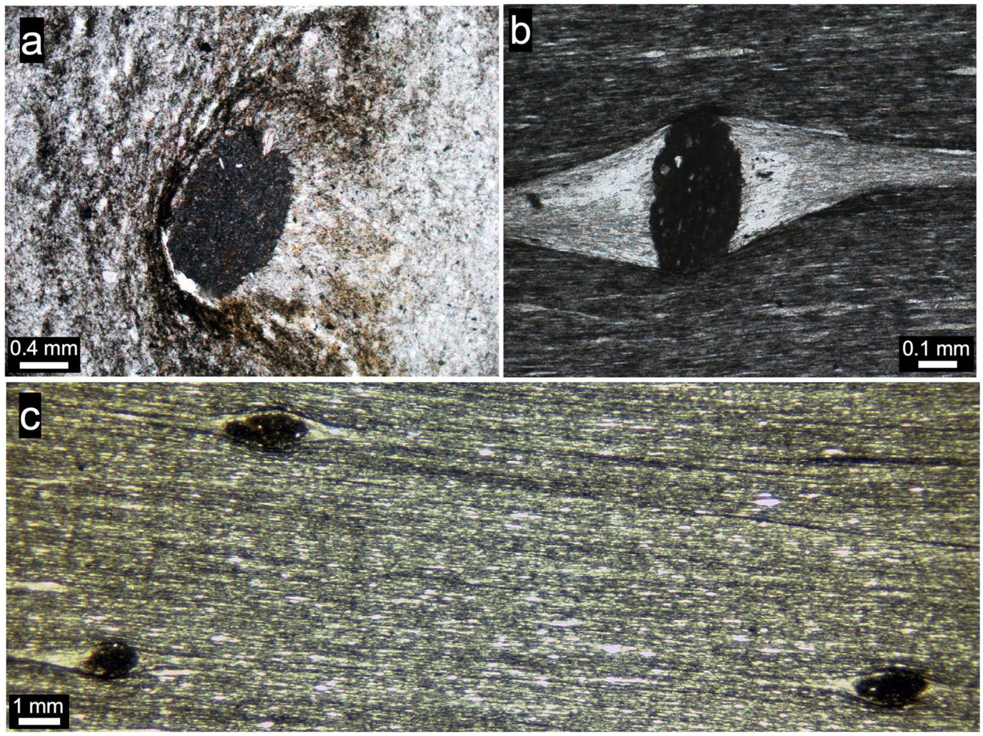

Fig. 8 Transmitted-light (PPL) images of nodular grey monazite from Middle Ordovician metasediments of the Navia-Alto Sil Domain (WALZ). The nodules occur within a low-grade matrix rich in organic matter depicting Variscan regional slaty cleavage (S_1). **a** Anllarinos (locality 10 in Fig. 6) showing selective formation of monazite within a pelitic, organic-rich layer richer adjacent to a sandy level; **b-c** Luarca beach (locality 11 in Fig. 6); monazite grains (up to three in c) showing variable development of pressure shadows formed by rotation (**b**) or flattening (**c**) depending on the initial orientation of monazite relative to compressive stress

monazite: notably lower Th and higher Nd concentrations compared to typical yellow monazite.

Whole sample analyses of Matamulas grey monazite via XRF and ICP-AES confirm the enrichment in Nd, Sm and Eu, together with low Th content. Elevated Si, Al, Fe and K reflect abundant mineral inclusions (Table 2; Supplementary Information). These results align with earlier reports for grey monazite from NW Iberia (Vaquero Nazábal 1979) and other global occurrences (Rosenblum and Mosier 1983; Tuduri et al. 2023).

In situ analyses, covering both monazite in original rocks and derived alluvial deposits from Lower Paleozoic metasediments (e.g., Belgium, Wales, Brittany; Burnotte et al. 1989; Milodowski and Zalasiewicz 1991; Tuduri et al. 2023) or younger units (Permian of Siberia, Lazareva et al. 2018; Triassic of Iran, Alipour-Asll et al. 2012; Cretaceous of Belgium, Cobert et al. 2015) reveal strong chemical zonation as an ubiquitous feature, even though most studies reported data for a selection of REE.

Grey monazite from Matamulas shows composition and zoning patterns comparable to those elsewhere. Nodules have Nd- and MREE-enriched cores, reaching up to 26.5 wt % Nd_2O_3 and 11.5 wt % Sm_2O_3. Concentric zoning of REE is generally continuous, occasionally oscillatory (Fig. 3c and e) and independent of surface colour. Other elements quantified (Th, Al, Ca, etc.) are very low and variable, showing no systematic trends.

The Ce_apfu vs. Nd_apfu diagram (Fig. 9a) indicates a continuum from Nd-rich cores to Ce-rich rims, with most analyses plotting on the monazite-(Ce) field (Tuduri et al. 2023). Larger and medium grains show a rimward drop in both Ce and Nd, suggesting replacement by other LREE (Fig. 9a). In fact, although as shown by Figs. 9 and 10, not only Nd but also Sm and Gd are replaced initially by Ce, it is La the element that progressively replaces other REE of lesser ionic radius towards rims. Pr exhibits a distinct trend: increasing from inner to outer core, then decreasing towards the rim (Fig. 10e). This decoupling of Pr may indicate early-stage liberation from other mineral during nodule growth, similar to observations in Brittany, interpreted as evidence that cores crystallised under lower-grade conditions than rim overgrowths (Tuduri et al. 2023).

The origin of these REE trends is unclear but may reflect progressive changes in fluid chemistry from complexation-controlled to sorption-controlled during nodule growth (Bau 1991). Initially, stable carbonate complexes ($LuCO_{3+}$ > $LaCO_{3+}$) and phosphate released from oxidizing organic matter promote MREE/HREE enriched cores, with REE being released from the surface of smectites and amorphous oxide minerals. Later, REE desorption from more stable phases (e.g., detrital mafics attested by the widespread presence of coarse chlorite grains) and from the HREE-depleted clays or oxides shifts the fluid composition toward LREE, forming the rim overgrowths. The absence of Eu anomalies suggests that feldspars were not significant during monazite formation.

Lanthanide + Y patterns normalized to European Shale composite (EUS) (Fig. 11) further illustrate zonation. Core

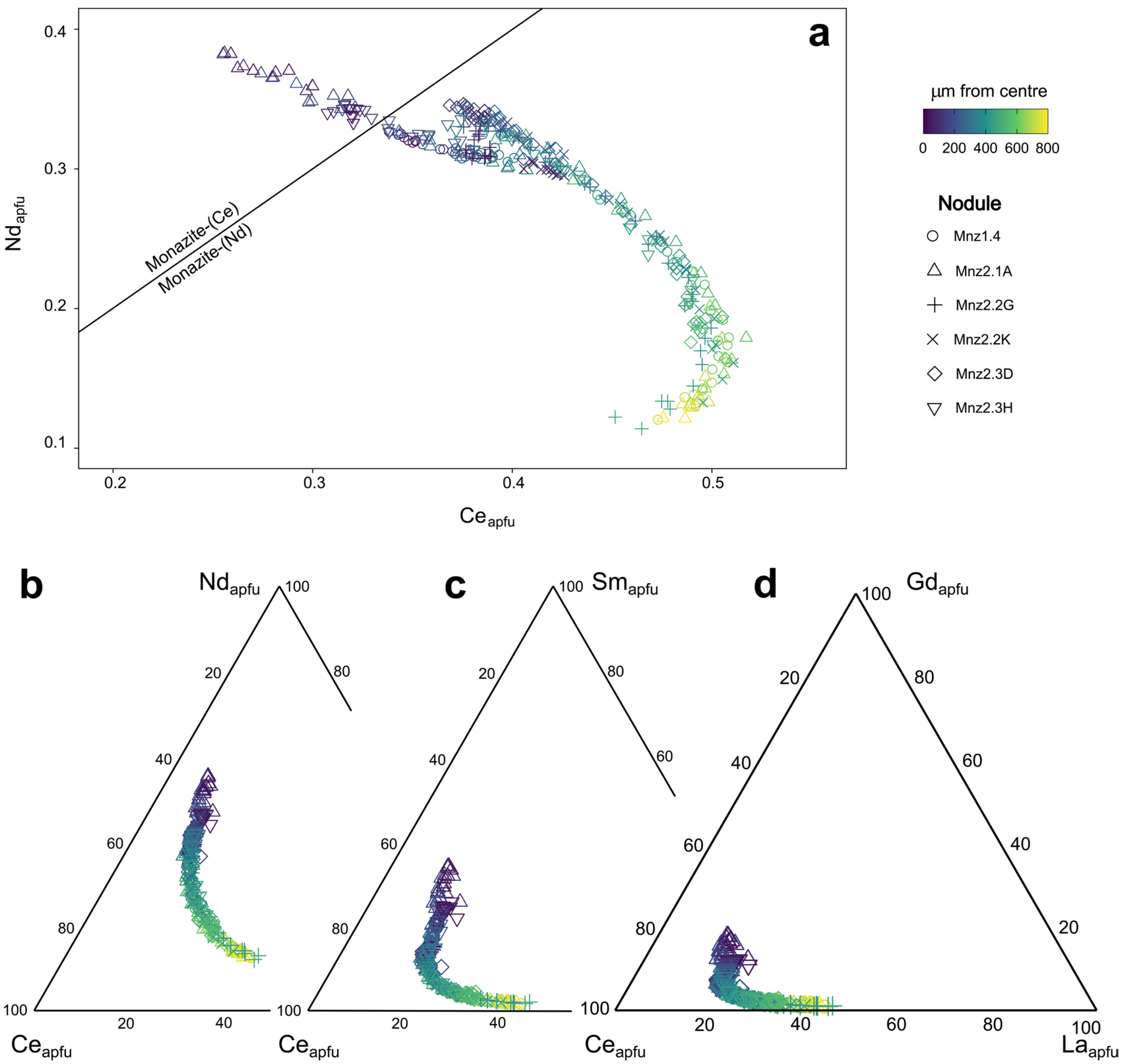

Fig. 9 **a** Nd and Ce zoning from core to rim in monazite from Matamulas of different sizes and colours (diagram after Tuduri et al. 2023). Mnz1.4 and Mnz2.1 A: grey and large-size grains; Mnz2.3D and Mnz2.3D: yellowish and medium-size grains; Mnz2.2G and Mnz2.2 K: reddish and small-size grains. **b** to **d** Progressive initial replacement of Nd, Sm and Gd by Ce, mainly in larger monazite, followed by an overall rimward increase in La in grains of different sizes and colours (same sample groups as above)

patterns display right-skewed bell-shapes with enriched in MREE, peaking at Sm, with moderate fractionation (mean $La_N/Lu_N = 92$; dark blue lines in Fig. 11a and f). Rim compositions are more variable. Large nodules exhibit continuous LREE-enriched trends without Eu anomaly (mean $La_N/Lu_N = 418.8$; yellowish lines of Mnz1.4 and Mnz2.1 A; Fig. 11a and b), while smaller grains show nearly flat LREE patterns, also without Eu anomaly (greenish lines of Mnz2.3D and Mnz2.3 H; Fig. 11e and f) with fractionation only from MREE to HREE (mean $La_N/Lu_N = 272.3$).

Thorium distribution is particularly relevant for industrial exploitation, as radioactive contamination is a major concern with yellow monazite. Grey monazite from Matamulas contains very low Th. EPMA data indicate that many spots are below detection limits, while LA-ICP-MS line scans reveal localized Th enrichments (as inferred from EDX images, Fig. 4b and d). EPMA-derived ThO_2 ranges from 0.01 to 0.40 wt %, and LA-ICP-MS yields a poorly constrained average of 0.43 wt % ThO_2 (includes occasional spikes up to ca.1.9 wt % ThO_2). Although such values are

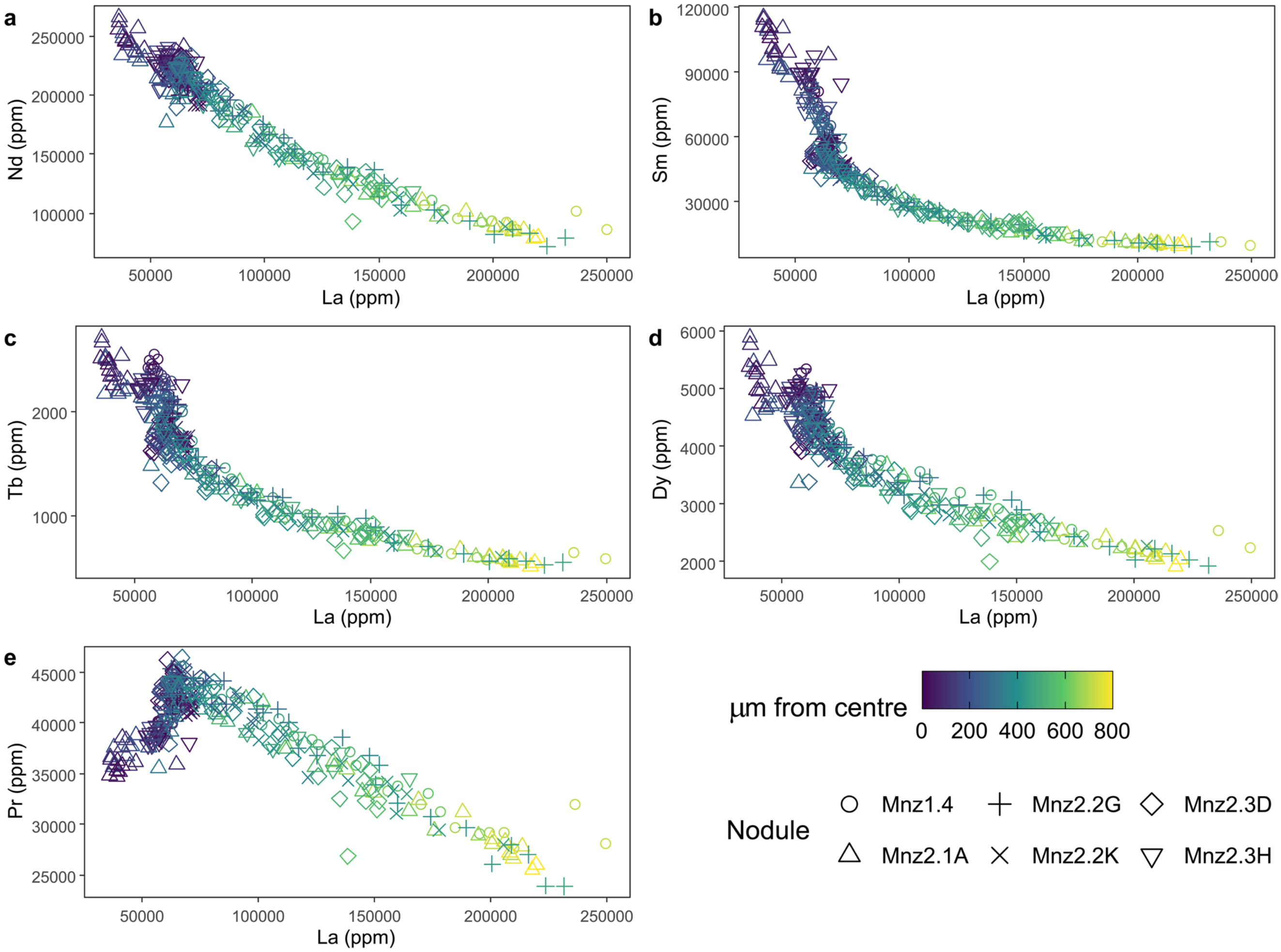

Fig. 10 **a** to **e** Generalized replacement of smaller-radius REE by La in monazite grains of different sizes and colours from Matamulas. **e** shows the shift in Pr ◊ Las substitution near the outer core. Mnz1.4 and Mnz2.1 A: grey and large-size grains; Mnz2.3D and Mnz2.3D: yellowish and medium-size grains; Mnz2.2G and Mnz2.2 K: reddish and small-size grains

largely below those typical of yellow monazite, none of them may be regarded as accurately representative of the Th content of grey monazite from Matamulas in view of the irregular distribution of this element. The average of 0.16 wt % ThO_2, obtained by means of whole sample analysis, is thus considered a more realistic estimation.

Timing of formation and structural relationships

Mineral inclusions in monazite studied frequently display rounded, corroded shapes, suggesting partial replacement by host monazite, and commonly show a core-to-rim concentration gradient, being more abundant toward the rims. While the inclusions generally lack a preferred orientation, some appear broadly aligned parallel to the long axis of the elliptical nodule sections. The relic orientation of inclusions is considered to reflect an anisotropy inherited from the original bedding (S_0). These microstructural observations support the hypothesis that the nodules grew in a variably compacted sedimentary matrix prior to regional metamorphism and the main Variscan deformation.

Field and thin-section observations (Figs. 7c, 8b and c and 12a; Supplementary Figs. 9a, 9b) indicate that nodule orientations and eccentricities relative to S1 cleavage are variable: the main axis of nodules may be parallel, oblique, or perpendicular to S_1. The surrounding cleavage in the matrix is locally deflected around the nodules, demonstrating that their flattened ellipsoidal shape predated deformation. The presence of large and sometimes oblique-to-S_1 pressure shadows indicate rigid rotation during the development of S_1 without significant shape change. Nodular grey monazite was thus fully developed prior to cleavage formation during the Upper Carboniferous.

The U-Pb geochronological data support this pretectonic origin. Ages from different nodules (ca. 399–402 Ma), together with the lack of disturbed analyses, suggest that the monazite was formed in relatively rapid event ca. 400 Ma ago. This occurred at an intermediate date between the

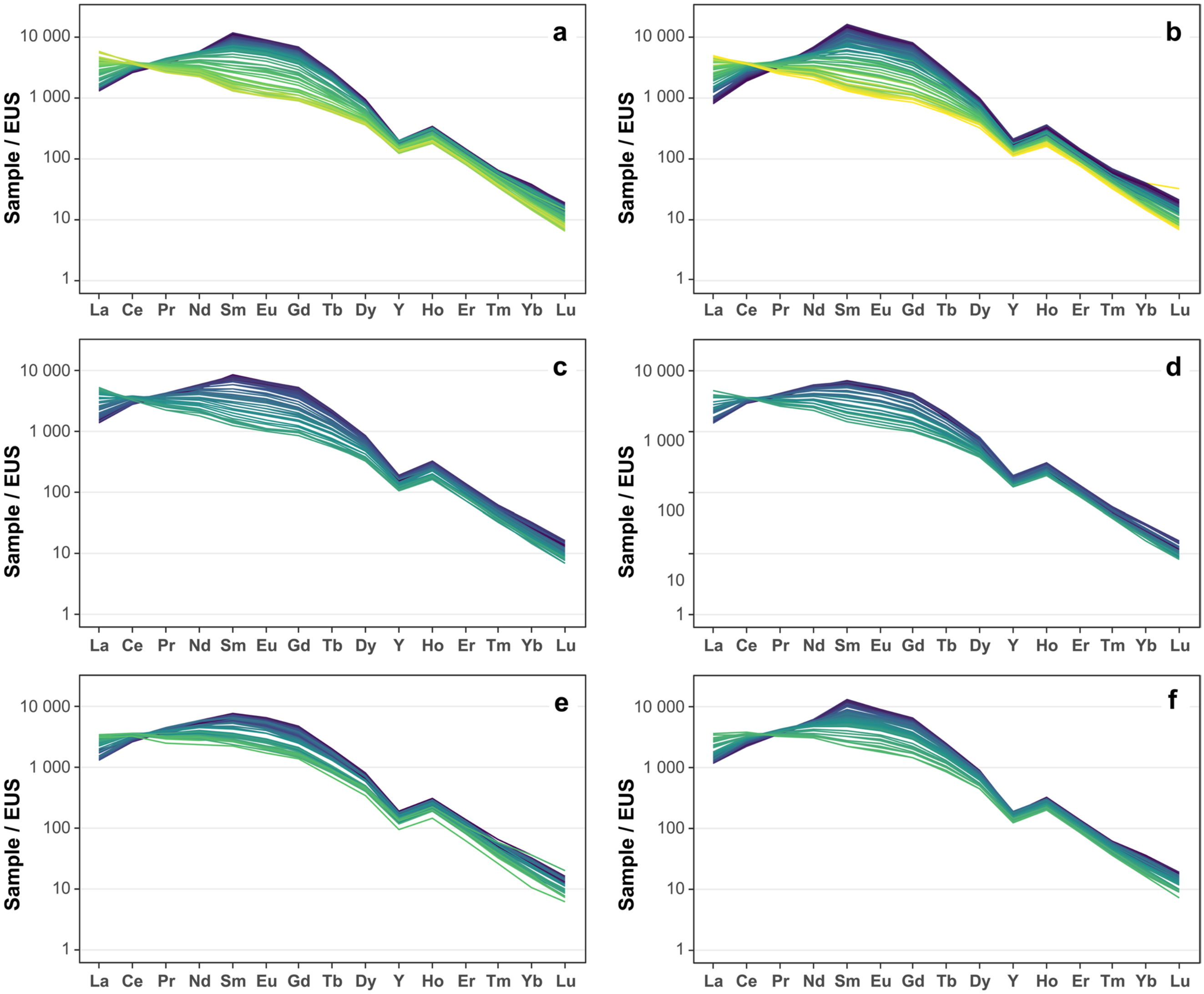

Fig. 11 EUS-normalizzed lanthanide+Y patterns for large (**a**, **b**), medium (**c**, **d**) and small monazite nodules (**e**, **f**). Cores show right-skewed patterns, whereas smaller nodules display fractionated to flat LREE-MREE patterns

deposit of the sediments (468 to 458 Ma) and the post-Serpukhovian (upper Carboniferous, ca. 323 Ma) development of the regional slaty cleavage (S_1). These results are consistent with the date obtained by Tuduri et al. (2023) for their Type-1 monazite (403.6 ± 2.9 Ma) from Ordovician black shales of the Armorican Massif (France), which is comparable to the nodular grey monazite of Matamulas. Both results are also in line with the date of 419 ± 14 Ma reported by Evans et al. (2002) for grey monazite from organic-rich Silurian metasediments of central Wales (Great Britain). Thus, nodular monazite was formed prior to the regional orogenic events, that is, before the Variscan tectono-thermal events in the Armorican and Iberian Massifs, and before the Caledonian events in Wales. In consequence, the monazite must have grown under diagenetic conditions when the sediment was in an early stage of consolidation.

During initial growth, a nodule could envelop up to > 50 vol % of surrounding matrix components (Fig. 12a and b), which may exhibit corrosion due to replacement by monazite. This early growth inherited the sedimentary fabric, reflected in variable inclusion orientations. The overall random orientation and flattened ellipsoidal morphology of the nodular monazite, observed both in thin sections and outcrops, likely reflects fluid-assisted growth along S_0 anisotropy, later coincident with S_1.

The increased concentration of phyllosilicate and other mineral inclusions towards the rims of some nodules (Fig. 2e) suggests localized fluid-assisted mobilization and refining during nodule growth. Moreover, optical zoning and cyclic twinning textures (Figs. 2c and 7c) point to progressive recrystallisation of precursor gels or cryptocrystalline aggregates into fully developed grey monazite. By the

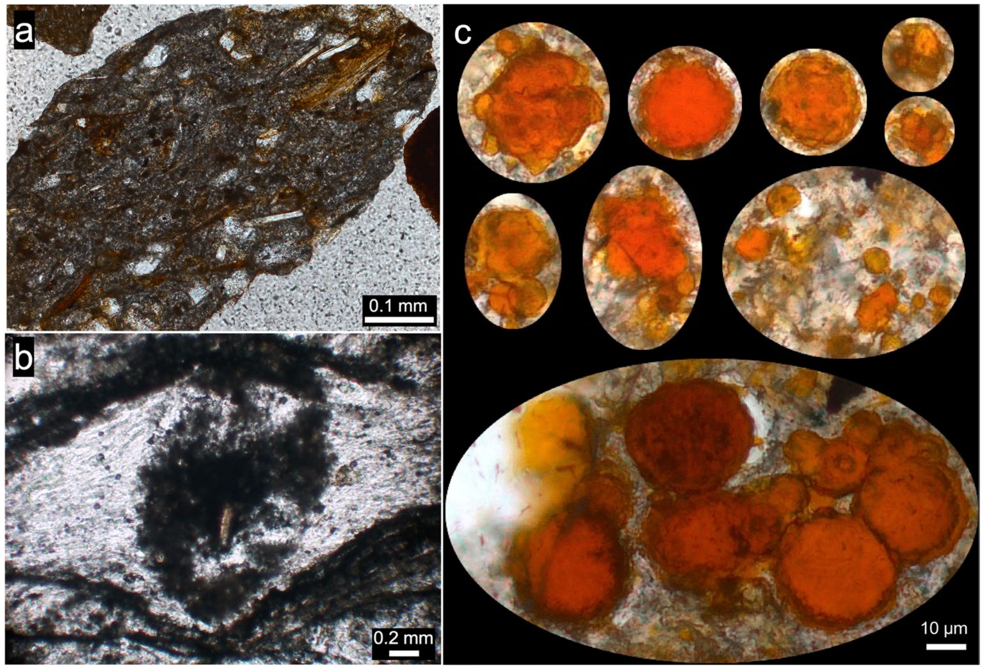

Fig. 12 Transmitted-light (PPL) images of early stages of nodular monazite formation. **a** panned nodule from Matamulas (locality 2 in Fig. 6) showing ≥ 50 vol % silicate inclusions (muscovite/sericite, chlorite, quartz, biotite relics, opaques). **b** in-situ, pre-kinematic nodule within slate from Anllarinos (locality 10 in Fig. 6) showing fragments of the matrix and poorly defined rims. **c** Transmitted-light (PPL) details of spherical Fe-oxide inclusions, probably replacing framboidal pyrite, within grey monazite from the Matamulas placer deposit (see Fig. 1 in Supplementary). Ochre spheroids and clusters may correspond to bacteriomorphic structures (Zhmodik et al. 2024)

time of Variscan deformation, most pre-kinematic, poikiloblastic nodules were already dense and rigid, producing the observed assortment of pressure shadows and fringe patterns associated with either rotation (Fig. 8b) or flattening (Fig. 8c) depending on the initial orientation of the monazite relative to the principal stress direction.

Conditions and mechanisms of formation

The temperature of formation of nodular grey monazite has been roughly estimated between 200 and 350 °C, corresponding to high-grade diagenesis up to the high-grade anchizone/epizone transition (Tuduri et al. 2023 and references therein). Recent reviews by Zi et al. (2024) compared low-temperature (< 350 °C) metamorphic and hydrothermal monazite with that from carbonatites, magmatic, and high-temperature metamorphic rocks. By their low Th and Ca, high REE content, and low Th/U, ThO_2 vs. Th/U and ThO_2 vs. UO_2 ratios, the composition of Matamulas monazite is consistent with hydrothermal and low-temperature metamorphic monazite (Janots et al. 2012; Taylor et al. 2015; Zi et al. 2024).

The exact determination of crystallization temperature is challenging. Indirect constraints come from regional comparisons. Minimum conditions can be inferred from the absence of nodular monazite within Middle Ordovician metapelites in the CZ (foreland and thrust belt of the Orogen). Using conodont colour alteration, illite crystallinity, clay-mineral assemblages and rock fabrics, García-López et al. (1997) estimated ca. 210 °C for the diagenesis/anchizone transition. In the Montes de Toledo area NW of Matamulas, organic reflectance and illite crystallinity indicate maximum recrystallisation temperature of 275 °C for the De Río Slates (Windle 1994). This suggests a temperature window of ca. 210–275 °C for nodular monazite formation in Middle Ordovician slates. In an attempt to refine these results, we have applied empirical and semiempirical formulations of chlorite thermometers (Verdecchia et al. 2019) to both Windle's (1994) and our own data. The results for matrix chlorite (S_1) and chlorite inclusions in grey monazite are similar, 272 °C and 268 °C as average, respectively. This suggests the re-equilibration of chlorite inclusions, but the high uncertainties (2SE > 60 °C) in both cases preclude definitive conclusions. In any case, given that monazite nodules already behaved as rigid concretions by the stage of S_1 development, these values place an upper-temperature limit for the growth of the nodules. The formation of nodular monazite probably was not a quick event, and their growth should certainly span a range of temperatures from, at least, that of breakdown of feldspar and formation of illite (60–120 °C; Awwiller 1993) to the mentioned upper limit.

Regarding the upper limit of stability of grey monazite, several authors have pointed out its breakdown under prograde metamorphism, becoming unstable at higher anchizone or greenschist facies conditions (Lacomme et al. 1993; Rosenblum and Mosier 1983; Tuduri et al. 2023). This pattern holds for Middle Ordovician slates in the Iberian Massif where grey monazite occurs exclusively in metapelites of lower grade than the biotite zone. Although the precise temperature of disappearance is unknown, it has been observed to coexist with matrix chloritoid (Vaquero Nazábal 1979) implying that grey monazite was still stable at ≥280 °C, the temperature of formation of chloritoid in metapelites (Bucher 2023).

Concerning the mechanisms of formation of grey monazite in shaly metasediments, several hypotheses have been put forward, from in situ recrystallisation of detrital yellow monazite to monazite saturation and precipitation involving fluid-assisted REE desorption from either clay minerals, Fe oxides/hydroxides or biogenic components (summaries in Tuduri et al. 2023; Zi et al. 2024). At Matamulas, burial of Ordovician sediments certainly caused temperature increase and fluid release, but the specific sources of REE and P or the reactions that produced monazite remain uncertain. A single mechanism is unlikely, and multiple processes may have acted during diagenesis. A compilation of chemical data from Ordovician shales of the Iberian Massif (Barba et al. 2011) shows a generalised low Ca content (0.22 CaO wt %), along with REE concentrations similar to European Shale (EUS; Bau et al. 2018): ΣREE_{EUS} = 246 ppm; $\Sigma REE_{Middle\ Ordovician}$ = 276 ppm. These values are similar to the mean of 243 ppm obtained by Windle (1994) for interbedded shale/sandstone or shale/siltstone from the base of the Ordovician up to the Middle Ordovician De Río Slates (where the nodular monazite occurs). Therefore, the black slates hosting grey monazite are not enriched in REE, implying REE remobilization was required for monazite formation. Windle (1994) also analysed the content of organic carbon in the same samples (ca. 0.5 wt %) and concluded that in such a reducing environment of sedimentation, there was no correlation of organic carbon content with the abundance of monazite. Instead, nodules correlated with higher K, Rb, Ba and Si in silty beds, which suggests a significant role of detrital micaceous components as REE source. A biogenic source may be considered for P, whose concentration in the De Río Slates, 2600 ppm, is distinctly higher than in shales elsewhere, such as 1700 ppm in the 'metamorphosed shale composite' of Gromet et al. (1984). Likewise, a correlation between Ca and P in the Montes de Toledo area suggests the presence of apatite, probably as a phosphoric cement produced during early diagenesis. Thus, it can be envisaged that in a Ca-poor matrix and a reducing environment of sedimentation, the apatite, whose stoichiometry limits the amount of REE in it, would destabilise during diagenesis and/or anchimetamorphism, with Ca being replaced by the REE for the formation of monazite. REE mobility at a small scale might have been enhanced eventually through the liberation of F during the apatite breakdown. The organic matter might have stressed initial sorption and concentration of divalent europium in monazite, which would have become progressively enriched in other REE and self-purified during diagenesis.

The absence of additional geochemical data precludes further interpretation, although some additional facts may be hypothesised. For instance, in the present case, an origin by recrystallisation of detrital yellow monazite is unlikely, since yellow monazite cores have not been observed (it may be noted that detrital monazite is rare in the Middle Ordovician slates and typically euhedral, showing no signs of instability under diagenetic or low-grade metamorphic conditions). Also, the observed zoning, with LREE concentrated in the rims and the rest of REE in the cores, strongly suggests changes in fluid chemistry and/or fluid volume increase, possibly driven by phyllosilicates breakdown over the timespan of monazite growth. Finally, limonite inclusions (<2 µm to >30 µm), likely replacing Fe-sulphide framboids, suggest occasional microbial involvement, consistent with observations from Siberian Permian placers (Zhmodik et al. 2024).

Concluding remarks

Nodular monazite occurs in dark, Middle Ordovician, barely metamorphosed carbonaceous-terrigenous sediments across extensive stretches of the Central Iberian and West Asturian-Leonese Zones of the Iberian Massif. Erosion of these black slates, coupled to short-range transport, has generated deposits of alluvial, millimetre-sized monazite nodules in Quaternary sediments at multiple localities of the Iberian Peninsula. Some of these deposits, due to their high concentration of monazite, qualify as placers and indicate potential for the economic exploitation of rare earth elements.

The liberated nodules are predominantly greyish, but surface colours can range from yellow to black. They are invariably rich in silicate and opaque inclusions, which are generally unoriented, though some may exhibit alignment related to the original bedding anisotropy (S_0). Optical zoning is typically observed, reflecting variations in the abundance and nature of these inclusions. Occasional clear cores with inclusion-rich rims suggest a refining process during crystal growth.

Concentric chemical zoning of REEs is a pervasive feature, either continuous or with recurrences, and is independent of the surface colour of the nodule. Core-to-rim REE distribution correlates with nodule size, with rims of larger nodules exhibiting the highest normalized La/Lu ratios. Monazite cores are systematically enriched in MREE and HREE, while rims are dominated by LREE, particularly La and Ce, which progressively replace REEs of smaller ionic radius, except for Pr, which displays different behaviour in the inner core regions. Thorium concentrations are low and irregularly distributed at the micrometre scale. These patterns indicate a significant role of the fluid phase during monazite formation.

U-Pb geochronology of monazite from the Matamulas placer deposit constrains their formation to ca. 400 Ma (Early Devonian), well before the Upper Carboniferous Variscan metamorphism and development of regional tectonic foliation. By that time, the nodules were already rigid forming pressure shadows and fringes during deformation. The nodules grew with random orientations, exhibiting uniaxial oblate or triaxial ellipsoids shapes, likely controlled by fluid circulation parallel to bedding planes within specific levels of the sedimentary pile. Consequently, the formation process i.a. interpreted to have occurred under diagenetic or low-grade burial metamorphic conditions. Under higher-grade metamorphism, these same stratigraphic units no longer contain nodular monazite.

The distribution of nodular grey monazite extends across Darriwilian low-grade metasediments in western Europe and may continue eastward and into NW Africa according to paleogeographic reconstructions of Gondwana prior to Rheic Ocean closure. The Matamulas placer deposit exemplifies the potential for exploration of grey monazite in alluvial contexts, which could be particularly valuable given the increasing global demand for rare earth elements.

Supplementary Information The online version contains supplementary material available at https://doi.org/10.1007/s00126-026-01432-9.

Acknowledgements The authors thank the following individuals and institutions for their assistance: B. Ábalos (UPV/EHU) for insightful comments on the structural relationships of nodular monazite; G. Galán and M. L. Arboleya (Universitat Autònoma of Barcelona) for providing access to thin sections from the Navia-Alto Sil Domain; L. M. Rodríguez and A. Cuesta for their help with the samples at the Museum of Geology (University of Oviedo); L. González-Menéndez for providing access to archival documentation at the Spanish Geological Survey. Technical and human support from M. E. Sánchez Lorda and J. Sangüesa of the SGIker (UPV/EHU/ERDF, EU) is gratefully acknowledged. Constructive comments by J. M. Hanchar, an anonymous Reviewer and F. Tornos (Associate Editor) were greatly appreciated.

Author contributions All authors contributed to the conception and design of the study. The first draft of the manuscript was prepared by J. I. Gil Ibarguchi and Sonia García de Madinabeitia. All authors reviewed and approved the final version of the manuscript.

Funding Open Access funding provided thanks to the CRUE-CSIC agreement with Springer Nature. This work benefited from EPOS-NL Facility Access awarded to J. I. Gil Ibarguchi and supported by the Dutch Research Council (NWO). E. Ortega received research funding from Minas de Almadén y Arrayanes S.A. (MAYASA). E. Burkhalter serves as a consultant for Quantum Minería.

Declarations

Competing interests The authors have no competing interests to declare that are relevant to the content of this article.

References

Alía Medina M (1962) Relaciones genético estructurales de algunos tipos de mineralizaciones uraníferas españolas

Alipour-Asll M, Mirnejad H, Milodowski AE (2012) Occurrence and paragenesis of diagenetic monazite in the upper Triassic black shales of the Marvast region, South Yazd, Iran. Mineral Petrol 104:197–210. https://doi.org/10.1007/s00710-011-0186-2

Awwiller DN (1993) Illite/smectite formation and potassium mass transfer during burial diagenesis of mudrocks; a study from the Texas Gulf Coast Paleocene-Eocene. J Sediment Res 63:501–512. https://doi.org/10.1306/D4267B3B-2B26-11D7-8648000102C1865D

Barba P, Ugidos JM, González Clavijo E, Valladares MI (2011) Geochemical features of Ordovician Succession in the Central Iberian Zone (Spain). In: Gutiérrez Marco JC, Rábano I, García-Bellido D (eds) 11th International Symposium on the Ordovician System, Alcalá de Henares, Ordovician of the World. pp 49–54

Bau M (1991) Rare-earth element mobility during hydrothermal and metamorphic fluid-rock interaction and the significance of the oxidation state of europium. Chem Geol 93(3–4):219–230. https://doi.org/10.1016/0009-2541(91)90115-8

Bau M, Schmidt K, Pack A et al (2018) The European shale: an improved data set for normalisation ofrare earth element and yttrium concentrations in environmental and biological samples from Europe. Appl Geochem 90:142–149. https://doi.org/10.1016/j.apgeochem.2018.01.008

Boatner LA (2002) Synthesis, structure, and properties of monazite, pretulite, and xenotime. Rev Mineral Geochem 48:87–121. https://doi.org/10.2138/rmg.2002.48.4

Bucher K (2023) Petrogenesis of metamorphic rocks. Springer International Publishing, Cham

Burnotte E, Pirard E, Michel G (1989) Genesis of gray monazites; evidence from the paleozoic of Belgium. Econ Geol 84:1417–1429. https://doi.org/10.2113/gsecongeo.84.5.1417

Castroviejo R (2023) A Practical Guide to Ore Microscopy—Volume 1. Springer International Publishing, Cham, Switzerland, p 1020. https://doi.org/10.1007/978-3-031-12654-3

Cobert C, Baele JM, Boulvais P et al (2015) Grey monazite paleoplacers in Lower Cretaceous continental formations in the Mons Basin, Belgium. In: SGA 13th Biennial Meeting. pp 703–708

Cooper DC, Basham IR, Smith TK (1983) On the occurrence of an unusual form of monazite in panned stream sediments in Wales. Geol J 18:121–127. https://doi.org/10.1002/gj.3350180204

Donnot M, Guigues J, Lulzac Y, Magnien A, Parfenoff A (1973) Picot P (1973) Un nouveau type de gisement d'europium: la monazite grise à europium en nodules dans les schistes paléozoïques de Bretagne. Miner Deposita 8:7–18. https://doi.org/10.1007/BF00203346

European Commission, Grohol M, Veeh C (2023) Study on the critical raw materials for the EU 2023 – Final report. Publications Office of the European Union, Luxembourg. https://doi.org/10.2873/725585

Evans JA, Zalasiewicz JA, Fletcher I et al (2002) Dating diagenetic monazite in mudrocks: constraining the oil window? J Geol Soc London 159:619–622. https://doi.org/10.1144/0016-764902-066

Förster H-J (2018) Accessory minerals in felsic igneous rocks - part 9 monazite-(Ce), xenotime-(Y) and zircon from late-Variscan biotite and two-mica granites of the Aue-Schwarzenberg granite zone (Western Erzgebirge – Vogtland metallogenic province, Germany). GFZ Data Serv. https://doi.org/10.5880/GFZ.6.2.2018.001

Förster H-J, Harlov DE (1999) Monazite-(Ce)-huttonite solid solutions in granulite-facies metabasites from the Ivrea-Verbano Zone, Italy. Mineral Mag 63(4):587–594. https://doi.org/10.1180/minmag.1999.063.4.11

García-López S, Brime C, Bastica F, Sarmiento GN (1997) Simultaneous use of thermal indicators to analyse the transition from diagenesis to metamorphism: an example from the variscan belt of Northwest Spain. Geol Mag 134:323–334. https://doi.org/10.1017/S0016756897006882

González Clavijo E (2006) La Geología del sinforme de Alcañices Oeste de Zamora. Publisher: Instituto Universitario de Geología Isidro Parga Pondal - Área de Xeoloxía e Minería do Seminario de Estudos Galegos. ISBN: 84-933799-6-4. 238 pp

Gromet LP, Haskin LA, Korotev RL, Dymek RF (1984) The “North American shale composite”: its compilation, major and trace element characteristics. Geochim Cosmochim Acta 48:2469–2482. https://doi.org/10.1016/0016-7037(84)90298-9

Harlov DE (2015) Apatite: a fingerprint for metasomatic processes. Elements 11:171–176. https://doi.org/10.2113/gselements.11.3.171

Hey MH (1954) A new review of the chlorites. Mineralogical Magazine J Mineralogical Soc 30:277–292. https://doi.org/10.1180/minmag.1954.030.224.01

IGME (2009) Mapa geológico de España. Escala 1:50.000. Segunda serie - Primera Edición. Hoja 864:21–34. https://info.igme.es/cartografiadigital/geologica/Magna50Hoja aspx?language=es&id=864 Venta de Los Santos

IGME (2016a) Mapa geológico de España. Escala 1:50.000. Segunda serie - Primera Edición. Hoja 836/18–33. Mestanza. https://info.igme.es/cartografiadigital/geologica/Geo50Hoja.aspx?Id=836&language=es

IGME (2016b) Mapa geológico de España. Escala 1:50.000. Segunda serie - Primera Edición. Hoja 838:20–33. Santa Cruz de Mudela. https://info.igme.es/cartografiadigital/geologica/Geo50Hoja.aspx?Id=838&language=es

Janots E, Berger A, Gnos E et al (2012) Constraints on fluid evolution during metamorphism from U-Th-Pb systematics in alpine hydrothermal monazite. 855 Chem Geol 326–327:61–71. https://doi.org/10.1016/j.chemgeo.2012.07.014

Junta de Extremadura (2019) Recursos mineros de Extremadura. Las rocas y minerales industriales. Mérida

Kremenetski AA, Leal GE, Amor JM, Potapova GY (1993) Eu-bearing monazites in black schists and associating placers: Composition, structures, genesis, economic aspects. In: Abstracts of Rare earth minerals: chemistry, origin and ore deposits, IGCP project 282 and 314. London, pp 61–62

Lacomme A, Hottin AM, Laval M (1993) La monazite grise du massif de L’Arize (Pyrénées françaises). Report R37041 GEO-SGN 93. Orleans

Lazareva EV, Zhmodik SM, Prokopiev AV et al (2018) Nodular monazite from placers in the Kular ridge (Arctic Siberia, Russia): composition and age. Russ Geol Geophys 59:1330–1347. https://doi.org/10.1016/j.rgg.2018.09.010

Ling M-X, Liu Y-L, Williams IS et al (2013) Formation of the world’s largest REE deposit through protracted fluxing of carbonatite by subduction-derived fluids. Sci Rep 3:1776. https://doi.org/10.1038/srep01776

Lozano Letellier A, González-Menéndez L, Gómez Fernández F et al (2023) Influencia de Los Minerales accesorios En Las Tierras raras de Pizarras Ordovícicas (Fm. Luarca, sinclinal de Truchas, León, España). Geogaceta 74:39–42. https://doi.org/10.55407/geogaceta98044

Martínez Catalán JR, Martínez Poyatos D, Bea F (Coords.), de Geología JA, Vera (eds) (2004) Geological Society of Spain-Geological Survey of Spain (SGE-IGME), Madrid, 68–69

Martínez Catalán JR, Schulmann K, Ghienne J-F (2021) The Mid-Variscan allochthon: keys from correlation, partial retrodeformation and plate-tectonic reconstruction to unlock the geometry of a non-cylindrical belt. Earth Sci Rev 220:103700. https://doi.org/10.1016/j.earscirev.2021.103700

Milodowski AE, Zalasiewicz JA (1991) Redistribution of rare earth elements during diagenesis of turbidite/hemipelagite mudrock sequences of Llandovery age from central Wales. Geol Soc Lond Spec Publ 57:101–124. https://doi.org/10.1144/GSL.SP.1991.057.01.10

Mohanty AK, Sengupta D, Das SK, Saha SK, Van KV (2004) Natural radioactivity and radiation exposure in the high background area at Chhatrapur beach placer deposit of Orissa, India. J Environ Radioact 75(1):15–33. https://doi.org/10.1016/j.jenvrad.2003.09.004

Overstreet WC (1967) The geologic occurrence of monazite. United States Geol Surv Prof Paper 530:338–pp

Pownceby MI et al (2019) Characterisation of phosphorus and other impurities in goethite-rich iron ores–possible P incorporation mechanisms. Miner Eng 143:106022. https://doi.org/10.1016/j.mineng.2019.106022

Ramsay JG (1967) Folding and fracturing of rocks. McGraw-Hill, New York

Rodríguez Fernández LR, López Olmedo F, Oliveira JT et al (2015) Geological map of Spain and Portugal 1:1.000.000. Madrid. https://info.igme.es/cartografiadigital/geologica/Geologicos1MMapa.aspx?Id=Geologico1000_(2015)&language=en

Rosenblum S, Mosier EL (1983) Mineralogy and occurrence of europium-rich dark monazite. United States Geological Survey Professional Paper, No. 1181,67pp

Salgueiro R, Inverno C, de Oliveira DPS et al (2020) Alluvial nodular monazite in Monfortinho (Idanha-a- Nova, Portugal): regional distribution and genesis. J Geochem Explor 210:106444. https://doi.org/10.1016/j.gexplo.2019.106444

Santos JJA, Conceição H, Leandro MVS, Rosa MdeLdaS (2018) Formation of monazite-(Ce, La) by fluid- apatite interaction: the Floresta Azul Alkaline Complex, Bahia, Brazil. Braz J Geol 48:721–733. https://doi.org/10.1590/2317-4889201820180069

Stacey JS, Kramers JD (1975) Approximation of terrestrial lead isotope evolution by a two-stage model. Earth Planet Sci Lett 26:207–221. https://doi.org/10.1016/0012-821X(75)90088-6

Taylor RD, Goldfarb RJ, Monecke T et al (2015) Application of U-Th-Pb phosphate geochronology to young orogenic gold deposits: new age constraints on the formation of the grass Valley gold District, Sierra Nevada foothills Province, California. Econ Geol 110:1313–1337. https://doi.org/10.2113/898econgeo.110.5.1313

Tuduri J, Pourret O, Gloaguen E et al (2023) Formation of authigenic grey monazite: a palaeo-thermal anomaly marker in very-low grade metamorphic rocks? Ore Geol Rev 160:105583. https://doi.org/10.1016/j.oregeorev.2023.105583

Vaquero Nazábal C (1976) Prospección y estudio mineralométrico de yacimientos detríticos: Aplicación del método en el Batolito de los Pedroches. PhD Thesis printed in 1977 by ENADIMSA EDICIONES, Serie 5, Trabajos de Tesis, nº6, 212 pp

Vaquero Nazábal C (1979) Descubrimiento monacita de facies aberrante. Boletín Geológico Y Min 374–379

Veerasamy N, Murugan R, Kasar S, Inoue K, Kavasi N, Balakrishnan S, Arae H, Fukushi M, Sahoo SK (2021) Geochemical characterization of monazite sands based on rare earth elements, thorium and uranium from a natural high background radiation area in Tamil Nadu, India. J Environ Radioact 232:106565. https://doi.org/10.1016/j.jenvrad.2021.106565

Verdecchia SO, Collo G, Zandomeni PS et al (2019) Crystallochemical indexes and geothermobarometric calculations as a multiproxy approach to P-T condition of the low-grade metamorphism: the case of the San Luis Formation, Eastern Sierras Pampeanas of Argentina. Lithos 324–325:385–401. https://doi.org/10.1016/j.lithos.2018.11.021

Vergara Espuelas R (2015) Tierras raras: trabajos de investigación en el yacimiento de monacitas de Matamulas. Ingeopres: Actualidad técnica de ingeniería civil, minería, geología y medio ambiente 245:36–42

Vergara Espuelas R (2019) Minería, Mercados y precios de Las Tierras raras. Semin Soc Esp Mineral 13:67–77

Windle SJ (1994) The genesis of grey monazite. PhD Thesis, University of Southampton

Zemel VK (1936) Analysis of monazites from the Aldan and Southern Yenisei gold placers. Zh Prikl Khim IX:1969–1971

Zhmodik SM, Rozanov AYu, Lazareva EV et al (2024) Signatures of the involvement of microorganisms in the formation of nodular monazite (kularite), Republic of Sakha (Yakutia), Russia. Dokl Earth Sci 516:995–1003. https://doi.org/10.1134/S1028334X24601494

Zi J-W, Muhling JR, Rasmussen B (2024) Geochemistry of low-temperature (<350°C) metamorphic and hydrothermal monazite. Earth Sci Rev 249:104668. https://doi.org/10.1016/j.earscirev.2023.104668